Posted on 11 Sep 2023 — The copyright holder is the author/funder. All rights reserved. No reuse without permission. — https://doi.org/10.22541/essoar.169447469.92501989/v1 — This a preprint and has not been peer reviewed. Data may be preliminary.

Free infragravity waves on the inner shelf: Observations and Parameterizations at two Southern California beaches

Athina MZ Lange[1], Julia W Fiedler[2], Mark A. Merrifield[3], and R.T. Guza[3]

[1]Scripps Institution of Oceanography, UC San Diego
[2]UCSD
[3]Scripps Institution of Oceanography

September 11, 2023

Abstract

Co-located pressure and velocity observations in 10-15m depth are used to estimate the relative contribution of bound and free infragravity (IG) wave energy to the IG wave field. Shoreward and seaward going IG waves are analyzed separately. At the Southern California sites, shoreward propagating IG waves are dominated by free waves, with the bound wave energy fraction <30% for moderate energy incident sea-swell and <10% for low energy incident sea-swell. Only the 5% of records with energetic long swell show primarily bound waves. Consistent with bound IG wave theory, the energy scales as the square (frequency integrated) sea-swell energy, with a higher correlation with swell than sea energy. Seaward and shoreward free IG energy is strongly tidally modulated. The ratio of free seaward to shoreward propagating IG energy suggests between 50-100% of the energy radiated offshore is trapped on the shelf seaward of 10-15m and redirected shoreward. Remote sources of IG energy are small. The observed linear dependency of free seaward and shoreward IG energy on local sea-swell wave energy and tide are parameterized with good skill (R2 ˜ 0.90). Free (random phase) and bound (phase-coupled) IG waves are included in numerically simulated timeseries for shoreward IG waves that are used to initialize (˜ 10m depth) the numerical nonlinear wave transformation SWASH. On the low slope study beach, wave runup is only weakly influenced by free shoreward propagating waves observed at the offshore boundary (foreshore slope = 0.02).

Free infragravity waves on the inner shelf: Observations and Parameterizations at two Southern California beaches

A.M.Z. Lange[1], J.W. Fiedler[1], M.A. Merrifield [1], and R.T. Guza[1]

[1]Scripps Institution of Oceanography, La Jolla, CA, USA

Key Points:

- Infragravity (IG) waves on the inner shelf (10-15m depth) in San Diego, USA are usually dominated by refractively trapped free waves.
- Seaward and shoreward propagating free IG energies are parameterized as a function of tide level and local sea-swell conditions.
- On a low slope (0.02) beach, numerical modeled wave runup is weakly influenced by the shoreward IG waves observed at the offshore boundary.

Corresponding author: Athina M.Z. Lange, alange@ucsd.edu

Abstract

Co-located pressure and velocity observations in 10-15m depth are used to estimate the relative contribution of bound and free infragravity (IG) wave energy to the IG wave field. Shoreward and seaward going IG waves are analyzed separately. At the Southern California sites, shoreward propagating IG waves are dominated by free waves, with the bound wave energy fraction $< 30\%$ for moderate energy incident sea-swell and $< 10\%$ for low energy incident sea-swell. Only the 5% of records with energetic long swell show primarily bound waves. Consistent with bound IG wave theory, the energy scales as the square (frequency integrated) sea-swell energy, with a higher correlation with swell than sea energy. Seaward and shoreward free IG energy is strongly tidally modulated. The ratio of free seaward to shoreward propagating IG energy suggests between 50-100% of the energy radiated offshore is trapped on the shelf seaward of 10-15m and redirected shoreward. Remote sources of IG energy are small. The observed linear dependency of free seaward and shoreward IG energy on local sea-swell wave energy and tide are parameterized with good skill ($R^2 \sim 0.90$). Free (random phase) and bound (phase-coupled) IG waves are included in numerically simulated timeseries for shoreward IG waves that are used to initialize ($\sim$ 10m depth) the numerical nonlinear wave transformation SWASH. On the low slope study beach, wave runup is only weakly influenced by free shoreward propagating waves observed at the offshore boundary (foreshore slope = 0.02).

Plain Language Summary

Infragravity (IG) waves are long-period (every 25 sec to 2.5 min) waves that contribute to coastal flooding and beach erosion. IG waves, generated near the shoreline by short-period sea-swell (SS) wave groups (known by surfers as "sets"), have long wavelengths (100s of m) and do not curl and break like ordinary sea and swell waves. Instead, they can bounce off the beach face and propagate seaward. Our study concerns IG waves on the inner shelf ($10 - 15$m depth, $\sim 500 - 700$m offshore), seaward of the region of IG generation. Similar to previous observations in Hawai'i and North Carolina, we find most of the bounced, seaward going IG energy cannot reach deep water and is trapped on the continental shelf. We develop an observation-based estimate IG wave energy on the inner shelf as a function of SS wave energy and tide level. Finally. we show with a numerical model that IG wave runup at the shoreline is influenced only weakly by IG waves on the inner shelf.

1 Introduction

Infragravity (IG) waves are low-frequency surface-gravity ocean waves with periods typically between 25-200s, longer period than the sea-swell waves that generate them. IG waves were first observed (Munk, 1949; Tucker, 1950) seaward of the surfzone, traveling shoreward with the group velocity of short-period wind-generated waves and $\sim 10\%$ of their amplitude. IG waves can contribute significantly to runup (Huntley, 1976; Guza & Thornton, 1982; Ruggiero, 2004; Stockdon et al., 2006, and many others), sediment transport (Aagaard & Greenwood, 1994, 2008; Baldock et al., 2010; De Bakker et al., 2016), harbor seiches (Okihiro et al., 1993; Ardhuin et al., 2010) and earth hum (Rhie & Romanowicz, 2006; Webb, 2007).

Shoaling, shoreward propagating sea-swell (SS) frequencies interact and transfer energy to their sum (higher-order harmonics) and difference (infragravity) frequencies through nonlinear triad interactions (Hasselmann et al., 1963; Elgar & Guza, 1985; van Dongeren et al., 2007). 'Bound waves' are shoreward propagating IG waves that are 180° out of phase with the envelope of higher-frequency sea-swell waves (Longuet-Higgins & Stewart, 1962). As shoaling SS waves become increasingly nondispersive, the bound wave approaches resonance, lags behind the wave group, and is eventually a 'free' wave (on the dispersion curve) that propagates to shore (List, 1986; Battjes, 2004; A. T. M. de

Bakker et al., 2015). Throughout the short wave (e.g. sea-swell) surf zone, free shoaling IG waves can acquire and lose energy from SS waves and can potentially break. At the shoreline, free IG waves can reflect and propagate seaward (Battjes, 2004; Thomson et al., 2006; S. M. Henderson et al., 2006; van Dongeren et al., 2007; Ruju et al., 2012; A. de Bakker et al., 2014).

In many locations, incident SS waves are relatively well characterized with buoys (Behrens et al., 2019), satellites (Ribal & Young, 2019; Qin & Li, 2021), and regional or global (e.g. WAVEWATCH III) wave models. While these SS waves can be used in offshore boundary conditions (BC) for surf zone models, typically in $\sim 10-20$m depth, the contribution of IG waves is not accurately observed or predicted by these systems. IG waves, typically observed with bottom-mounted pressure and/or current sensors, are less widely observed and characterized (Okihiro et al., 1992; Ardhuin et al., 2014; A. J. Reniers et al., 2021). The practical limitations of direct observations of infragravity waves motivates the present efforts to parameterize IG energy for use in nearshore models. Bound wave theory has been implemented as an offshore IG boundary condition in laboratory studies where the wavemaker is carefully controlled to create only a shoreward propagating bound IG wave and (ideally) to absorb seaward propagating IG waves (van Noorloos, 2003; Van Thiel De Vries et al., 2008; G. Ruessink et al., 2013; Altomare et al., 2020, and resulting papers). The offshore boundary condition in field settings have included theoretical bound waves and also observed timeseries (Roelvink et al., 2009; Zijlema, 2012; A. de Bakker et al., 2014; A. T. M. de Bakker et al., 2015; Dusseljee et al., 2014; Rijnsdorp et al., 2014, 2015; Fiedler et al., 2019; Zhang et al., 2020; Li et al., 2020; C. S. Henderson et al., 2022). The effect of free shoreward propagating IG waves in the model offshore boundary has received little attention, and no existing parameterization includes both 2D bound and free IG waves. Here, 3 years of pressure and current (PUV) data in 10-15m depth are used to determine (and parameterize) the variation of incident IG waves with a range of SS waves. A parametric offshore IG boundary condition is developed.

1.1 Bound Waves

Bound infragravity spectral energy $E_{IG}^{bound} = \int_{IG} \mathbf{E}^{bound}(f)df$ is estimated from second-order nonlinear wave theory (Hasselmann, 1962; Sand, 1982; Herbers, Elgar, & Guza, 1995, and many others).

$$\mathbf{E}_{IG}^{bound}(\Delta f, \Delta\theta) = 2\int_{\Delta f} D^2 S(f,\theta_1)S(f+\Delta f,\theta_2)df, \tag{1}$$

$$\begin{aligned} D &= \quad \frac{-gk_1k_2\cos(\Delta\theta)}{2\omega_1\omega_2} + \frac{1}{2g}(\omega_1^2+\omega_2^2+\omega_1\omega_2) + C\frac{g(\omega_1+\omega_2)}{(gk_3\tanh(k_3h)-(\omega_1+\omega_2)^2)*\omega_1\omega_2}, \\ C &= \quad (\omega_1+\omega_2)*\left(\frac{\omega_1\omega_2}{g}\right)^2 - k_1k_2\cos(\Delta\theta) - \frac{1}{2}\left(\frac{\omega_1k_2^2}{\cosh^2(k_2h)} + \frac{\omega_2k_1^2}{\cosh^2(k_1h)}\right), \end{aligned}$$

with wavenumber k, angular frequency ω $(= 2\pi f)$ and where the sea-swell frequency-direction spectra $S(f,\theta)$ can be estimated from a PUV, a pitch-roll buoy (Kuik, 1988), or a regional wave model. The interaction coefficient D is computed for the difference frequency (Δf) of every frequency pair (f_1, f_2) and if assuming directionally spread waves (2D), every difference direction $(\Delta\theta = \theta_2-\theta_1+180°)$. D varies strongly as a function of $\Delta\theta$, depth, and SS frequency f. In shallow water, D is maximum (D_{max}) for co-linear $(\Delta\theta = 0)$ waves, and 1D theory $(\Delta\theta = 0)$ is the upper limit on bound wave energy. D decreases quickly with increasing $\Delta\theta$; $\Delta\theta = 30°$ results in $D \sim 25\% D_{max}$ (Herbers & Guza, 1994). The theoretical sensitivity of 2D bound wave energy to $S(f,\theta)$ and the fundamentally low resolution of a single PUV directional estimator limits the accuracy of the present 2D bound wave estimates. The coupling coefficient is frequency dependent and swell $(8-25\text{s})$ produces larger bound waves than sea $(4-8\text{s})$ (Okihiro et al., 1992).

Bound IG waves can alternatively be estimated with the third-order spectrum (bispectrum, Hasselmann et al., 1963; Kim et al., 1980; Elgar & Guza, 1985) that depends on nonlinear phase coupling between wave triads with angular frequencies ω_1, ω_2, ω_{1+2}. The bispectrum is the expected value of the triple product of complex Fourier coefficients, $B(k,l) = \tilde{E}[X_k X_l X_{k+l}]$.

With random phases and no nonlinear coupling of the three frequencies, the bispectrum vanishes. The normalized magnitude of the bispectra ($\mathbf{b}$, bicoherence),

$$\mathbf{b}(f_1, f_2) = \frac{B(f_1, f_2)}{\sqrt{\mathbf{E}(f_1)\mathbf{E}(f_2)\mathbf{E}(f_1 + f_2)}}, \tag{2}$$

measures the strength of the phase coupling between the three waves. The bispectrum phase (biphase) corresponds to the phase lag between the IG wave and the SS wave group (Elgar & Guza, 1985). The forced wave spectral density is the bispectrum integrated over all frequency pairs for a given difference frequency (Herbers & Guza, 1994),

$$\mathbf{E}_{IG}^{forced}(\Delta f) = \alpha(\Delta f)|b_i(\Delta f)|^2 \mathbf{E}(\Delta f), \tag{3}$$

$$\mathbf{b}_i(\Delta f) = 2\int_{\Delta f}^{\inf} df B(f, \Delta f) / \sqrt{2\int_{\Delta f}^{\inf} df \mathbf{E}(f + \Delta f)\mathbf{E}(f)\mathbf{E}(\Delta_f)}, \tag{4}$$

and the bias term α can be computed from the bound wave theory.

1.2 Free Waves

Free waves contribute significantly to IG waves (Gallagher, 1971; Huntley et al., 1981; Oltman-Shay & Guza, 1987; Okihiro et al., 1992; Zijlema, 2012; Smit et al., 2018). 'Edge' waves are free waves trapped on a sloping beach by shoreline reflection and back-refraction by the increasing water depth (Eckart, 1951). Edge waves are sensitive to geography, with the amount of trapping depending on the continental shelf and beach topography (Herbers, Elgar, Guza, & O'Reilly, 1995). Seaward propagating IG waves that propagate freely from the shoreline across the shelf to deep water are known as 'leaky' waves (Webb et al., 1991; Ardhuin et al., 2014; Rijnsdorp et al., 2021). Ardhuin et al. (2014) and Rawat et al. (2014) parameterize seaward-going free wave energy (radiated from the surfzone) for use as an incident boundary condition for global model WAVEWATCH III, but the free IG wave climate on the inner shelf is poorly understood.

Previous work in Duck, NC, Southern California, and Hawai'i, USA and the North Sea have investigated the fraction of IG energy contained in the bound component, giving an indication of the amount of free shoreward wave energy. Numerous studies at Duck, NC ($\sim$ 8−13m depth) (Elgar et al., 1992; Herbers & Guza, 1994; B. G. Ruessink, 1998; A. J. H. M. Reniers, 2002) found that the bound wave fraction was typically between 10−20%, with higher values above 30% (and up to 100%) only during the most energetic SS conditions. In the North Sea ($\sim$ 30m depth), IG wave conditions are always free wave dominant and only during the peak of storms is the fraction bound $\geq$ 50% (A. J. Reniers et al., 2021). At beaches in Southern California and Hawai'i ($\sim$ 8−13m and 183m depth) (Okihiro et al., 1992), up to 50% of the IG energy is at times attributed to bound wave energy. The bound fraction is dependent on water depth; Elgar et al. (1992) observed twice the bound fraction in 8m depth compared to 13m depth in Duck, NC. Torrey Pines has long been a study site for refractively trapped waves (Huntley et al., 1981; Guza & Thornton, 1985; Oltman-Shay & Guza, 1987; Oltman-Shay & Howd, 1993; Thomson et al., 2006), with significant trapped IG energy detected shoreward of 15m water depth. This refracted energy then propagates onshore as free waves. These trapped waves are not phase-coupled to local (instantaneous) SS wave groups because they are not generated locally in space or time.

In this study, we analyze the relative contribution of bound and free IG energy to the total IG energy in $10-15$m water depth for beaches in San Diego County, USA, confirm theoretical estimates of the incident bound wave energy, investigate parameterizations for both bound and free IG energy and estimate an IG sea surface elevation timeseries that can be used as an incident boundary condition for nearshore models. Section 2.1 describes the dataset and quality control. Section 2.2 confirms that directional bound wave theory (Hasselmann, 1962) accurately predicts the observed bound wave energy. In Section 2.2 and 2.3, the relative contributions of shoreward propagating bound and free IG waves and their respective dependencies on the SS wave field are presented and compared with previous observations from other sites. The total incident bound and free IG energy and the spectral shape of the free energy are discussed in Section 3. Comparison to a previously developed seaward IG parameterization (Ardhuin et al., 2014), the tidal dependence and the effect of the IG BC in a phase-resolving nearshore numerical model on IG swash is presented in Section 4.

2 Observations

2.1 Data

Bottom-mounted pressure sensors and current meters (PUV) were deployed in 10 and 15-m depths at Torrey Pines State Beach and Cardiff State Beach, CA intermittently between Fall 2019 and Spring 2022 (Figure 1 and Table 1). Data were collected continuously between Fall 2021 and Spring 2022 as part of the Runup and Bathymetry 2D (RuBy2D) experiment at Torrey Pines, a 3km long, alongshore-uniform composite (summer sand, winter cobbles) beach. Cardiff is a 1.8km alongshore-variable beach, with a rocky reef beginning approximately 125m offshore at the southern end (Ludka et al., 2019). The 2 Hz PUV data were segmented into 3h records. The three largest tidal constituents are removed from the bottom pressure and velocity records, and the records are surface-corrected using linear finite-depth theory over the frequency band $0.004-0.25$ Hz. Computed spectra are segmented in 7200s demeaned ensembles, with an applied 50% overlapping Hanning window, with 0.0003 Hz frequency resolution and 13 degrees of freedom. The IG band is defined between $0.004-0.04$ Hz, the swell band between $0.04-0.12$ Hz and the sea band between $0.12-0.25$ Hz. As quality control, 3-hour pressure and velocity spectra passed a Z-test (Eq. 1 in Elgar et al., 2005),

$$Z^2 = \frac{P^2}{\left(\frac{\omega}{gk}\right)^2 \frac{\cosh^2 kh_P}{\cosh^2 kh_U}(U^2+V^2)}, \tag{5}$$

with cutoffs of $0.8 < Z_{IG} < 1.2$ and $0.95 < Z_{SS} < 1.05$. This confirms the use of linear theory in the sea surface correction. Additionally, only records with reflection coefficients (Eq. 4 in Sheremet et al., 2002) of $\mathscr{R}^2_{SS} < 0.25$ and $\mathscr{R}^2_{IG} < 2.5$ are used further. Only 5 values are removed with $\mathscr{R}^2_{IG} > 2.5$ with max $\mathscr{R}^2_{IG} = 2.9$. Details of the resulting 2494 quality controlled 3h records and SS bulk wave statistics are in Table 1. Spectral wave model (MOPS, O'Reilly et al., 2016) hindcast data from the observation periods show similar distributions of bulk parameters as a 23-year hindcast (Figure 2). The present observations are representative of the San Diego wave climate. Sea-surface elevation and velocity are combined to estimate shoreward and seaward propagating wave components, following Sheremet et al. (2002). Unless explicitly stated, the shoreward sea-surface elevation timeseries is used below to characterize the offshore boundary condition for wave propagation models.

2.2 Bound Waves

The 1D and 2D (±90° from shorenormal directionally-integrated) bound wave energies (Hasselmann, 1962) show the effects of directional spreading on the interaction

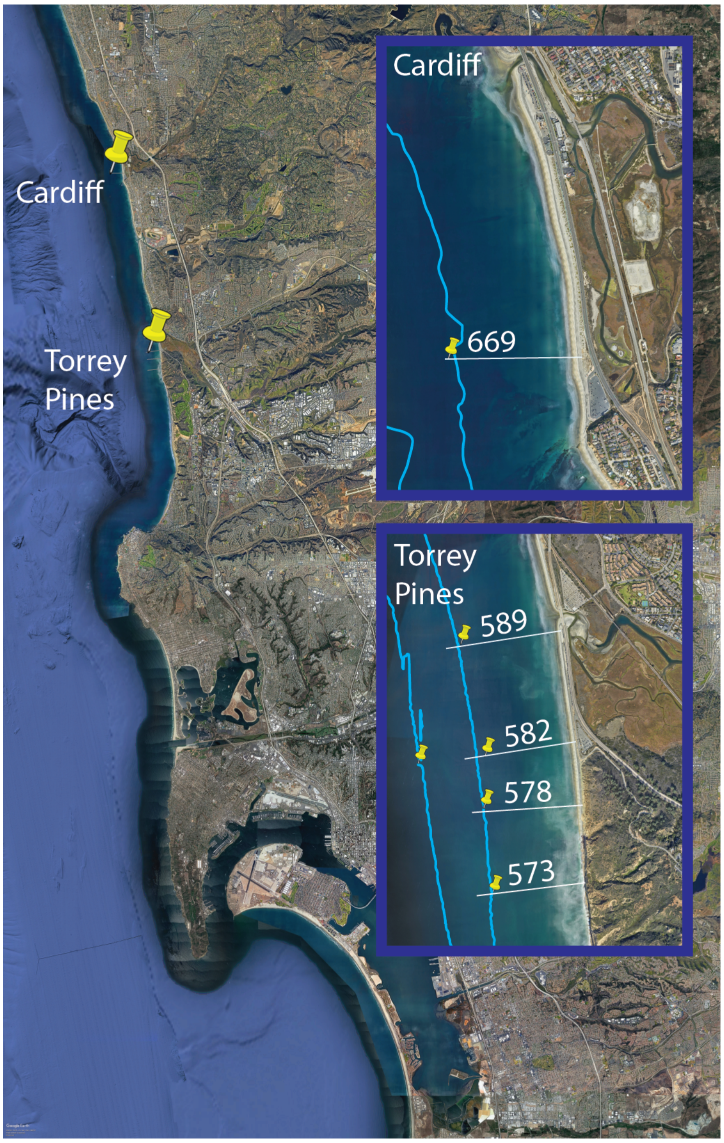

Figure 1. Co-located near-bottom pressure and biaxial acoustic current meter (PUV) in 10m and 15m depth at Torrey Pines and 10m depth at Cardiff. The Scripps Institution of Oceanography's wave MOnitoring and Prediction (MOP) (O'Reilly et al., 2016) transect numbers are given along with the 10 and 15m depth contours (NAVD88m).

coefficient D (Eq. 1 and Figure 3). The 1D estimates are about $\sim$ 3x larger than the directionally-integrated 2D estimates.

Bispectral analysis confirms 2D nonlinear theory (Hasselmann, 1962)(Figure 4). However, bispectral E_{IG}^{forced} estimates can be inaccurate when nonlinear coupling is weak, bound wave energy is low and free waves dominate. At individual frequencies, the bispectral and the bound wave estimates can differ by as much as a factor of 50 (Figure 3 and Herbers and Guza (1994)). Integrated over IG frequencies, the 2D bound wave and the forced wave energy (for fraction bound $>$ 15%) agree well ($R^2 = XX$, Figure 4). The cases of fraction bound $>$ 15% are typically larger SS events (back-refracted deep water wave height H_0 and wavelength L_0 give median $\sqrt{H_0 L_0} = 13.1$m, compared to

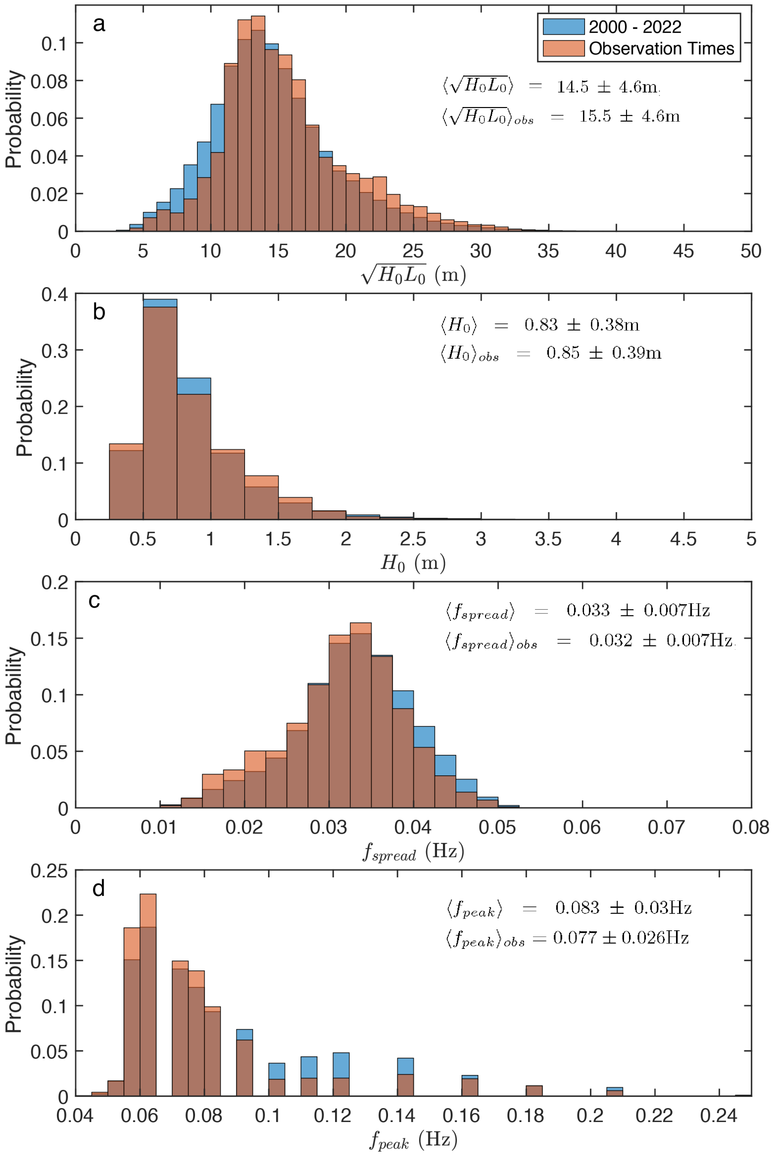

Figure 2. Histograms of (a) Offshore wave height H_0 and offshore wavelength L_0 in $\sqrt{H_0 L_0}$, (b) H_0, (c) frequency spread f_{spread}, and (d) peak frequency f_{peak} at Torrey Pines in 10m at MOP582. Histograms are similar for 2000 - 2022 hindcast (blue, 201,600 1h values) and present observations (orange, 12,602 1h records). Mean ± 1 standard deviation of the full 23 year hindcast and over the present observation time period (MOPS) are given.

MOP	Date	Depth (m)	Distance from backbeach (m)	# of records	H_{SS} (m)	T_p (s)	D_p (degrees)	D_{spread} (degrees)
582	11/19 - 04/20	10	580	316	0.3 - 2.4	5 - 21	0 - 23	7 - 21
582	10/20 - 03/21	10	580	315	0.3 - 4.1	5 - 21	0 - 25	9 - 22
582	07/21 - 09/21	10	580	223	0.4 - 1	5 - 19	0 - 29	14 - 24
669	07/21 - 09/21	10	600	285	0.4 - 1.1	5 - 20	1 - 32	6 - 25
573	10/21 - 03/22	10	600	281	0.4 - 2.5	5 - 19	0 - 28	8 - 22
578	10/21 - 11/21	10	630	55	0.4 - 1.7	9 - 20	1 - 10	10 - 22
582	10/21 - 02/22	10	630	323	0.3 - 2.3	5 - 20	0 - 19	9 - 21
582	10/21 - 02/22	15	1020	401	0.5 - 2.7	5 - 20	0 - 25	8 - 25
589	10/21 - 02/22	10	660	289	0.3 - 2.3	6 - 20	0 - 32	9 - 22

Table 1. PUV Bulk Statistics. MOP location (580s are Torrey Pines and 669 is Cardiff in O'Reilly et al. (2016); Ludka et al. (2019)), date range, depth, distance from backbeach to PUV, the number of records for each PUV, significant wave height H_{SS}, peak period T_p, peak direction D_p and spread D_{spread}.

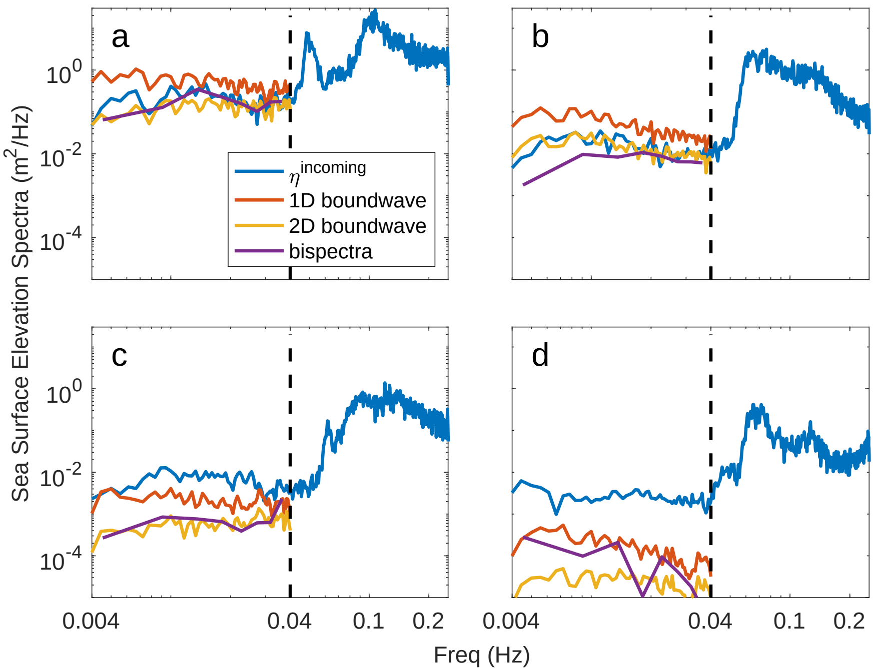

Figure 3. Observed (blue) sea surface elevation frequency spectra $\mathbf{E}(f)$ (d.o.f. = 30) in 10m for varying sea-swell wave heights H_{SS} (a) H_{SS} = 3.7m, $D_{spread,SS}$ = 18°, fraction bound = 74% (b) H_{SS} = 1.4m, $D_{spread,SS}$ = 13°, fraction bound = 100%, (c) H_{SS} = 1.0m, $D_{spread,SS}$ = 17°, fraction bound = 10%, and (d) H_{SS} = 0.4m, spread $D_{spread,SS}$ = 24°, fraction bound = 1%. In the IG band (f < 0.04 Hz, dashed vertical line), theoretical results are shown for 1D bound wave and 2 D bound wave, and for a bispectral approach (Herbers & Guza, 1994). Fraction bound (based on 2D bound waves) ranges from about 100% (a, largest H_{SS}) to 1% (d, smallest H_{SS}).

the median of the dataset = 10.7m). Analysis below uses 2D bound wave theory that (unlike bispectral estimates) does not rely on insitu IG observations and can be estimated from SS spectral waves from a buoy or wave model. Only 5% of the cases (120/2488) have a fraction bound greater than 50% (Figure 5 d). Similar to previous observations (Herbers, Elgar, & Guza, 1995; B. G. Ruessink, 1998) the fraction bound increases with increasing E_{IG} and E_{SS} and decreasing depth (or tide stage) (Figure 5 a). The frequency dependence of the bound wave coupling coefficient is seen with E_{IG}^{bound} being more highly correlated with E_{swell} ($R^2 = 0.84$) than E_{sea} ($R^2 = 0.59$) (Okihiro et al., 1992; Elgar et al., 1992).

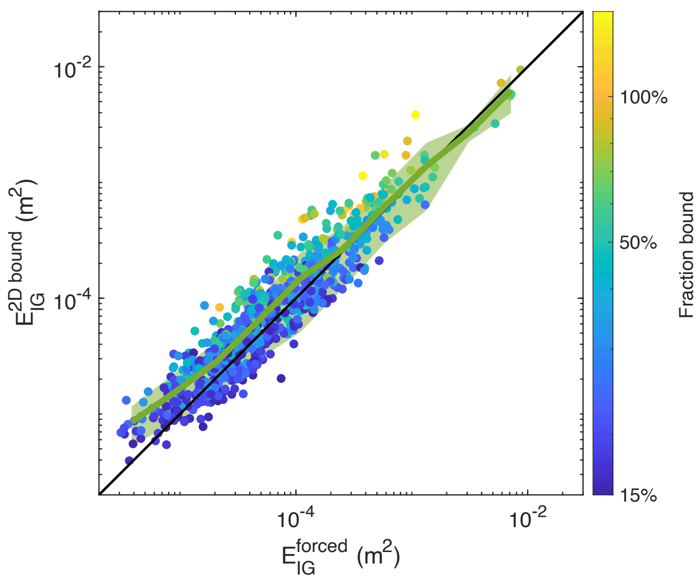

Figure 4. Bound IG energy from nonlinear 2D theory (Hasselmann, 1962) versus an estimate E_{IG}^{forced} based on bispectral analysis (Herbers & Guza, 1994). Colors are fraction bound based on 2D bound wave theory. When fraction bound < 15% bispectral results are widely scattered, and not shown or included in R^2. The 1-1 line, and mean and standard deviation for binned data (green curve and shading) are shown.

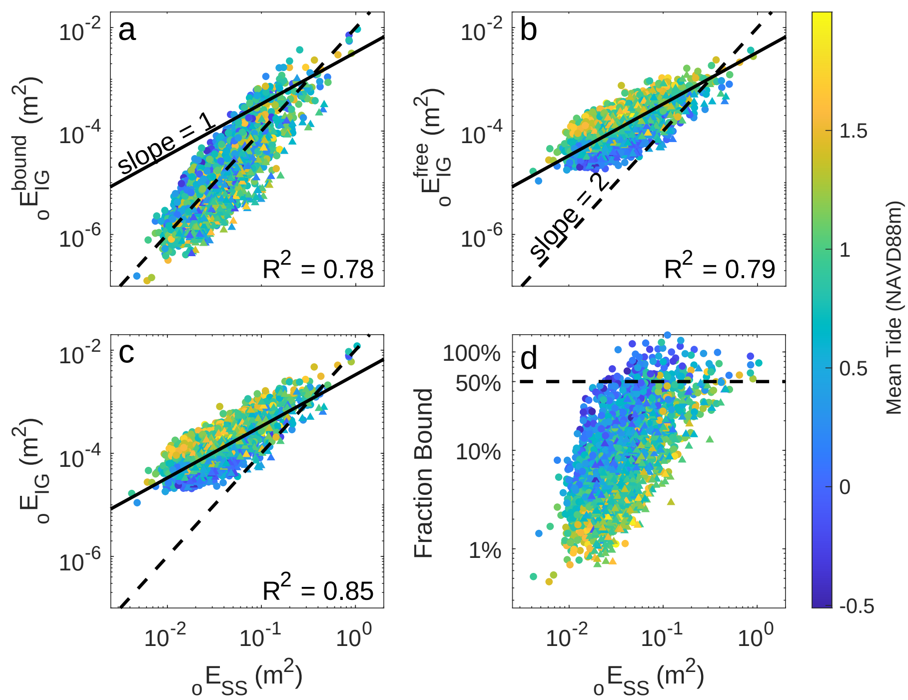

Figure 5. Observed shoreward propagating IG energy (a)E_{IG}^{bound}, (b) E_{IG}^{free}, (c) E_{IG}^{total}, and (d) fraction bound versus E_{SS}. Most observed fraction bound are < 50% (dashed horizontal line) and many are < 10%. △ is 15m PUV data. Correlations R^2 are given. E_{IG}^{bound} scales as E_{SS}^2 whereas both total and free IG energy scale as E_{SS}. In panels (a - c), the solid line shows a linear dependence on E_{SS} (slope = 1), and dashed line shows a quadratic dependence on E_{SS} (slope = 2).

2.3 Free Waves

The shoreward free IG energy spectra are estimated by subtracting the bound wave estimate ($\mathbf{E}_{IG}^{bound}(f)$) from the total shoreward IG energy spectra. These shoreward-directed free waves are a combination of refractively trapped (and typically locally generated) waves and leaky waves from remote sources. The free (and due to the dominance of free wave IG energy, the total) wave energy is approximately linearly proportional to E_{SS} (Figure 5 b, c, and consistent with Herbers, Elgar, Guza, & O'Reilly, 1995; Okihiro & Guza, 1995). This linear dependence on E_{SS}, as opposed to a quadratic dependence for the bound wave, has been attributed to dissipation (Herbers, Elgar, Guza, & O'Reilly, 1995). Free waves have a weaker depth dependence (h^{-1}) than bound waves (h^{-5}), consistent with Herbers, Elgar, Guza, and O'Reilly (1995).

Okihiro et al. (1992) estimated that in Southern California for typical SS energy, 25% of the IG energy was bound in 8-13m depth, 70% was trapped shoreward of a sensor in 183m depth, and only 5% was leaky. Leaky, free IG waves can propagate across ocean basins and in deep water appear uncoupled from and uncorrelated with local SS wave conditions (Webb et al., 1991; Ardhuin et al., 2014). However, on the inner shelf, remotely generated IG waves only dominate local IG waves when E_{SS} is very low (Herbers, Elgar, Guza, & O'Reilly, 1995; Sheremet et al., 2002). Remotely generated IG waves (i.e., unrelated to local SS wave energy) are not considered in the following analysis and contribute to parameterization noise.

3 Parameterizing the IG wave field

3.1 Bound Waves

Although 2D bound wave energy can be determined from the incident sea-swell spectrum, parameterizations of the total bound wave energy from bulk sea-swell wave statistics are convenient. Linear regression between ${}_{pred}E_{IG}^{bound}$ and $E_{SS}^2 h^{-5}$ (with exponents predicted in Herbers, Elgar, and Guza (1995) and similar to B. G. Ruessink (1998)), yields correlation coefficients R^2 between $0.58-0.91$, for 10m Torrey Pines, 15m Torrey Pines and 10m Cardiff PUVs. A frequency-weighted sea-swell energy integral $\left(\int_{SS} \mathbf{E}(f) f^{-1} df\right)$ (similar to the approach of Fiedler et al. (2020)) has higher correlations in all cases (Eq. 6 with $R^2 = 0.84 - 0.97$, 95% CI $[14.98, 15.37]$, Figure 6 a),

$$ {}_{p}E_{IG}^{bound} = 15.2 \left(\int_{SS} \mathbf{E}(f) f^{-1} df \right)^2 h^{-5}. \tag{6} $$

The units of the dimensional constant on the right-hand side are selected to yield m^2.

3.2 Shoreward Free Waves

Linear regression between ${}_{obs}E_{IG}^{free}$ and E_{SS} gives correlation $R^2 = 0.79$ (Figure 5). However, similar to the bound wave parameterization, a frequency-weighted SS energy integral increases the correlation ($R^2 = 0.84$). The observed tidal dependence of free IG energy is accounted for with the normalized tide

$$ \tilde{\sigma} = \frac{\text{tide}_{obs} - \text{tide}_{low}}{\text{tide}_{high} - \text{tide}_{low}}, \tag{7} $$

where 2.5m is the total tidal range observed across all deployments), with $\tilde{\sigma} = 0$ at the lowest observed tide (-0.5 NAVD88m), and $\tilde{\sigma} = 1$ at the highest tide (2 NAVD88m). Tide data is the 3h average obtained from a NOAA tide gauge (Station 9410230, La Jolla). Including a linear $\tilde{\sigma}$ dependence in the regression improves the correlation between observed and predicted total E_{IG}^{free} energy to $R^2 = 0.9$ (95% CI $[0.00066, 0.00068]$, Eq. 8, Figure 6 b) at all but the lowest tides and E_{SS},

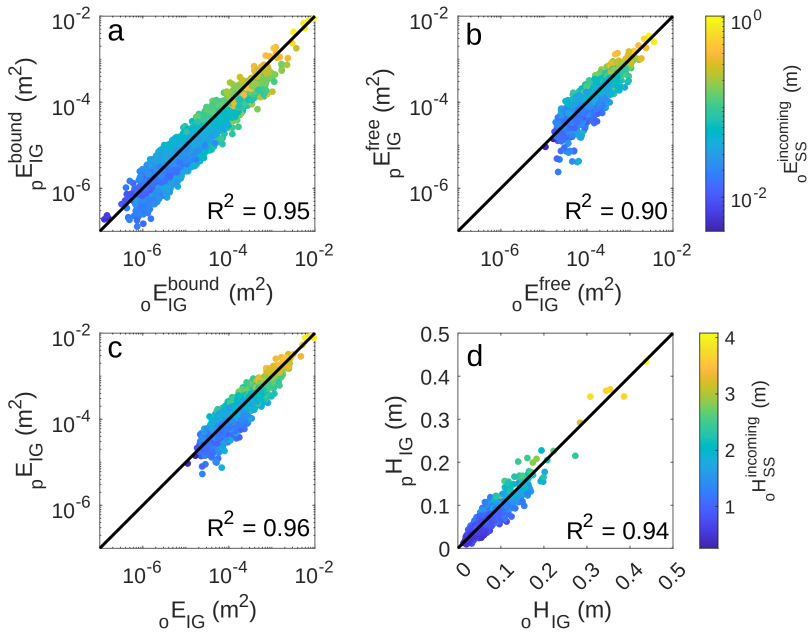

Figure 6. Parameterizations of incident IG wave field. (a) 2D bound wave parameterization (Eq. 6), (b) Free wave parameterization (Eq. 8), (c) 2D bound wave theory + free wave parameterization, colored by total incident SS energy (see color bar in (b)) and (d) significant wave height of estimated IG timeseries, colored by SS significant wave height.

	$\int_{SS} \mathbf{E}(f)df$	$\int_{SS} \mathbf{E}(f)f^{-1}df$	$\tilde{\sigma}\int_{SS} \mathbf{E}(f)f^{-1}df$
10m Torrey Pines	0.82	0.88	0.92
15m Torrey Pines	0.63	0.74	0.84
10m Cardiff	0.5	0.69	0.87
Total	0.79	0.84	0.9

Table 2. R^2 between total (frequency-band integrated) free shoreward IG energy observed and three parameterizations using the observed sea-swell wave energy spectrum $\mathbf{E}_{SS}(f)$. PUV sensors were deployed in 10m and 15m at Torrey Pines and 10m at Cardiff (see Table 1 for details). In all cases, $\tilde{\sigma}\int_{SS} \mathbf{E}(f)f^{-1}df$ has the highest R^2, where $\tilde{\sigma}$ is the relative tide level (Eq. 7).

$$_pE_{IG}^{free} = 0.00067\tilde{\sigma}\int_{SS} \mathbf{E}(f)f^{-1}df. \quad (8)$$

Correlations in different depths and beaches are given in Table 3.2.

The total shoreward IG energy, with contributions from both bound and free waves can be estimated with local SS parameters. The parameterization performs well ($R^2 = 0.96$) for all but the smallest E_{SS} and/or tides using either the bound wave parameterization (Eq. 6) or the integrated 2D Hasselmann bound wave energy (Figure 6 c). With the smallest E_{SS} and lowest tides, the parameterization underpredicts E_{IG} perhaps owing to free waves from remote sources (Webb et al., 1991; Ardhuin et al., 2014) and the inaccuracy of Eq. 6) when $\tilde{\sigma} = 0$.

Functional forms of the frequency distribution of the free IG energy were compared with the observed free IG spectra (normalized by the frequency-weighted SS energy). Forms investigated include linear and cubic fits to the median spectral shape, the spectral shape of Ardhuin et al. (2014) and an altered form (referred to as *nouvelleArdhuin*, Eq. 9),

$$A(f) = \begin{cases} \beta \frac{1}{\Delta f} * [f/0.012\text{Hz}] & \text{when } f < 0.012\text{Hz} \\ \beta \frac{1}{\Delta f} * [0.012\text{Hz}/f] & \text{when } f > 0.012\text{Hz} \end{cases}, \tag{9}$$

with $\beta = 0.0146$ (median spectral energy density at $f = 0.012$Hz).

NouvelleArdhuin has the smallest (~ 0.35) median root-mean-square logarithmic error (RMSLE) between ${}_{obs}E_{IG}^{free} * A(f)$ and ${}_{obs}\mathbf{E}_{IG}^{free}(f)$. Over all 2494 records, RMSLE are linear ~ 0.45, cubic ~ 0.40 and using Ardhuin et al. (2014) ~ 0.42. The free wave frequency distribution varies over a wide range and leads to relatively large RMSLE errors in all tested forms. NouvelleArdhuin (Eq. 9) is relatively simple, has the smallest errors, and is used below.

Timeseries realizations of the shoreward free IG are estimated from an inverse FFT of ${}_{pred}\mathbf{E}_{IG}^{free}(f)$,

$$\begin{aligned} {}_{p}\mathbf{E}_{IG}^{free}(f) &= {}_{p}E_{IG}^{free} * A(f), \\ {}_{p}E_{IG}^{free} &= 0.00067\tilde{\sigma} \int_{SS} \mathbf{E}(f) f^{-1} df, \end{aligned} \tag{10}$$

with random phases and $A(f)$ (Eq. 9).

Linearly combining the computed bound wave timeseries with the estimated shoreward propagating free wave timeseries (with random phase), yields an estimated total shoreward IG timeseries that can be used as a boundary condition for numerical models. The parameterizations approximately reproduce a range of infragravity heights (Figure 6 c, RMSE ~ 0.01m, Model skill = 0.82, $R^2 = 0.95$, Bias = 0.006m).

4 Discussion

Ardhuin et al. (2014) parameterized seaward free IG energy as a function of local sea-swell conditions, and used that parameterization as a shoreline boundary condition in a global ocean wave model. The assumptions that seaward IG energy is free, directionally broad, and mainly radiated from the surfzone underlie the parameterization ${}_{p}\mathbf{E}_{IG}^{sea}(f)$

$${}_{p}\mathbf{E}_{IG}^{sea}(f) = \left[1.2\alpha^2 \frac{kg^2}{c_g 2\pi f} \left(\frac{H_s T_{m,0}^2}{4} \right)^2 \right] * \frac{1}{\Delta f} \left[\min\left(1, \frac{0.015\text{Hz}}{f}\right) \right]^{1.5}, \tag{11}$$

with the first part determining the frequency-band integrated ${}_{p}E_{IG}^{sea}$ energy, and the second, the frequency distribution of the seaward IG spectrum. Zheng et al. (2021) compared output from the Ardhuin et al. (2014) model and observations of H_{IG} and found $R^2 = 0.6$. This approach, for seaward IG energy, yields similar parameters for α ($= 6.6 \text{ x } 10^{-4} s^{-1}$) with $R^2 = 0.71$ between estimated and observed E_{IG}^{free} (Figure 7 a). A parameterization, similar to Eq. 8, for the seaward energy,

$${}_{p}E_{IG}^{seaward} = 0.001\tilde{\sigma} \int_{SS} \mathbf{E}(f) f^{-1} df. \tag{12}$$

shows similar tidal dependence of seaward and shoreward energy, and similar high skill $R^2 = 0.91$ (Figure 7 b). The ratio of seaward/shoreward = 0.001/0.00067 = 1.5, is constant and independent of tide. Although the dependencies on $\tilde{\sigma}$ and the constant are not well constrained, the implication that $\mathscr{R}_{IG}^2$ is not a function of tide level is supported by the low correlation ($R^2 = 0.22$) between tide and $\mathscr{R}_{IG}^2$ (Figure 8).

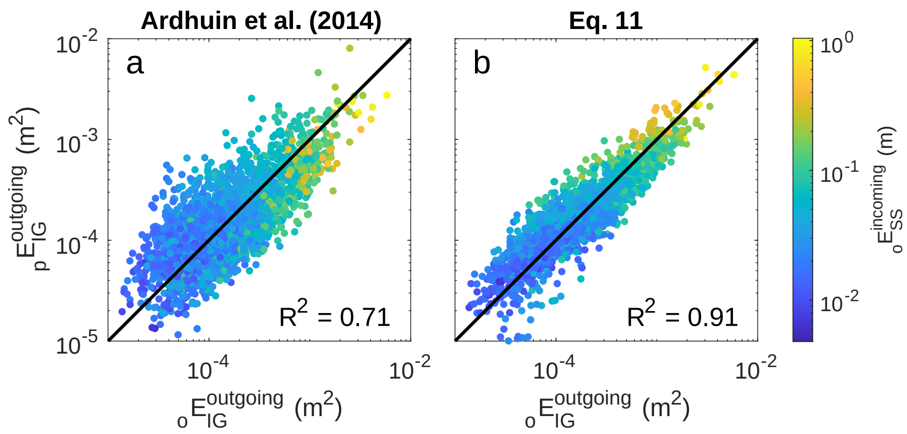

Figure 7. Parameterization of seaward IG energy from local SS conditions. (left) Ardhuin et al. (2014) ($R^2 = 0.71$) and (right) new parameterization ($R^2 = 0.91$), including tidal dependence (Eq. 12).

The observed total and free shoreward IG energy is tidally modulated(Figure 5 b, c), consistent with previous observations of total (seaward plus shoreward) IG energy in Southern California (Okihiro & Guza, 1995). This modulation, lower E_{IG} at low tide, has been attributed to IG energy loss within the surfzone being stronger on flat and shallow low-tide beaches than on steeper high-tide beaches (given a concave beach profile, Figure 8) (Thomson et al., 2006). Note that refractive trapping of seaward IG energy creates shoreward IG waves. That is, seaward and shoreward IG waves both increase at high tide, when the surfzone more efficiently radiates IG energy.

Observed values of $\mathscr{R}^2_{IG}$ vary between 0.5 - 2.5, whereas $\mathscr{R}^2_{IG} = 1.5$ follows from the present crude parameterizations. While $\mathscr{R}^2_{IG}$ at the shoreline is constrained to < 1, $\mathscr{R}^2_{IG} > 1$ in 10-15m depth can indicate IG surf zone generation and radiation, and shelf trapping. The ratio of free seaward to shoreward propagating IG energy in 10-15m depths is usually between 1 and 2. Along with the high correlation between E_{SS} and $_{obs}E^{free}_{IG}$, this suggests that between half and all of the energy radiated seaward is trapped on the shelf seaward of 10-15m and redirected shoreward (similar results seen in Gallagher, 1971; Elgar & Guza, 1985; Oltman-Shay & Guza, 1987; Okihiro et al., 1992; Elgar et al., 1992, 1994; Herbers & Guza, 1994; Herbers, Elgar, & Guza, 1995; Herbers, Elgar, Guza, & O'Reilly, 1995; Okihiro & Guza, 1995; Sheremet et al., 2002; Battjes, 2004; Thomson et al., 2006; S. M. Henderson et al., 2006; Rijnsdorp et al., 2015).

4.1 Numerical modelling of wave runup

The open-source, phase-resolving SWASH model (Zijlema et al., 2011) is used widely to simulate wave transformations and runup. SWASH successfully reproduces SS and IG evolution in laboratory channels with simple $h(x)$, and carefully controlled normally incident waves (A. de Bakker et al., 2014; Ruju et al., 2014; Suzuki et al., 2017). Field observations and model predictions of IG wave evolution and runup are also in good agreement, although limited by the relatively small range of conditions for which offshore boundary conditions (e.g. incident SS and IG waves), sandy beach bathymetry, and runup are all accurately known (Nicolae Lerma et al., 2017; Fiedler et al., 2018, 2019; Valentini et al., 2019; C. S. Henderson et al., 2022). For the current model runs, for computational reasons SWASH is run in nonstationary 2D mode in a narrow channel, with a curvilin-

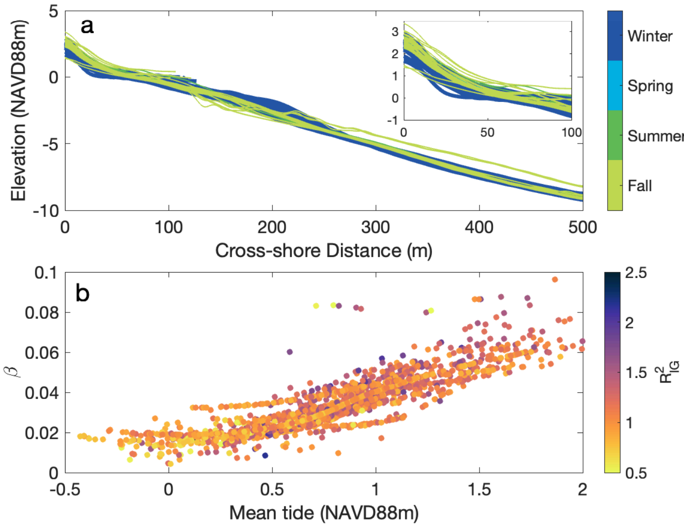

Figure 8. (a) Mean depth profiles at Torrey Pines (MOP 578 - 589), colored by season of survey. 85% of the 2209 surveys were collected in September/October/November ($n = 747$) and December/January/February ($n = 1125$). Insert shows subaerial beach. (b) Beach slope versus mean tide (relative to NAVD88m) of 3h record) at Torrey Pines. Beach slope is the linear fit ±0.5m around the tide level. The concave subaerial beach is steeper at high tide than low tide.

ear grid with a 2-m alongshore mesh for two identical parallel transects with 2 vertical layers. Waves are 1D. The normally incident wave field is prescribed with a Fourier series at the offshore boundary in 14m depth, about 600m from the shoreline. Parameter settings are as in Lange et al. (2022).

Significant IG growth and decay occurs during SS shoaling and breaking. Comparisons of runup with model run with $E_{IG} = 0$ and nouvelleArdhuin at the offshore boundary provide a measure of the effect of additional energy incident at the boundary. To test the relationship between incident IG energy in 10m and IG runup, we ran 23 wave cases of incident wave height ranging from $0.3 < H_{SS} < 4.1$m and $0.01 < H_{IG} < 0.44$m, with the IG boundary condition given by either $E_{IG} = 0$ or nouvelleArdhuin, and with the bathymetry profile either a 2-slope linear profile or an observed profile, for a total of 92 runs.

On the 2-slope profile, differences in runup with $E_{IG} = 0$ and nouvelleArdhuin are very small. On the observed bathymetry (derived from Figure 8 a), differences are detectable and best fit line slopes differ by about 15%. Consistent with linear intuition, runup is increased (modestly) by including incident IG waves at the offshore boundary. However, the cross-shore evolution of the shoreward IG waves is nonlinear and much more complicated than suggested by this simple example (Ruju et al., 2012; Fiedler et al., 2019; Mendes et al., 2018; Rijnsdorp et al., 2022). With steep test bathymetries and energetic wave conditions (not shown and not realistic in Southern California) $E_{IG} = 0$ can generate higher runup than nouvelleArduin, and effects of the offshore boundary condition on IG swash and runup can be significant (up to 20% different in the current cases and greater in cases run in Lange et al. (2022)).

We note that SWASH-modelled runup results were insensitive to different realizations of random phase in the simulations of free waves (not shown). Finally, SWASH-modelled seaward going IG energy in 10-15m was, for unknown reasons, significantly higher than the corresponding PUV observation (not shown), similar to C. S. Henderson et al.

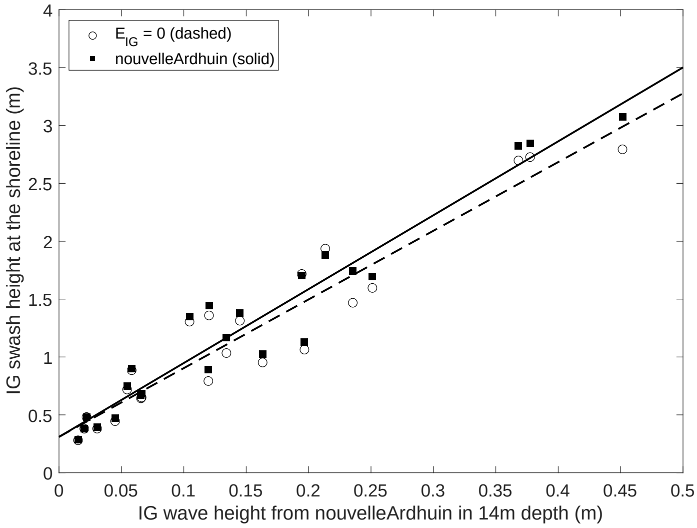

Figure 9. SWASH-modelled IG runup swash height versus nouvelleArdhuin offshore boundary condition IG height (∘, solid line is best fit). Runup is relatively insensitive to setting offshore $E_{IG} = 0$ (•, dashed). Best fit line slopes differ by 15% indicating a slight reduction in runup using $E_{IG} = 0$.

(2022). Possibly, errors arise because the SWASH 1D simulations assume normal wave incidence and do not support trapped waves. Simulations in 2D are beyond the present scope.

The applicability of the present results to other sites is unknown. Bound wave theory is general, not site-specific, and has no tunable parameters. However, the values of “free wave” parameters (Eqs. 6 and 10) are expected to vary with beach and shelf geometry. For example, the average depth of the North Sea is only 90m and slopes are low, potentially limiting the importance of refractive trapping relative to steeply sloped islands with deep water relatively close to shore (Rijnsdorp et al., 2021). The present sites are not between headlands or bounded by (fixed) offshore reefs. Selective amplification at particular IG frequencies has not been observed either in runup or on the inner shelf. Remotely generated IG waves from transoceanic sources are usually of relatively little importance. IG energy levels on the inner shelf depend on local waves and tide level. The numerical model result that IG wave runup at the shoreline is influenced only weakly by free IG waves on the inner shelf could significantly simplify overtopping forecasts by reducing the need for regional forecast models of IG waves.

5 Conclusion

The relative contribution of bound and free infragravity waves to the IG wave field on the inner shelf (depth $\sim 10-15$m) in San Diego County, USA was examined using PUV observations and nonlinear wave theory. In general, free waves dominate the IG wave field with only 5% of the records showing a bound wave fraction $> 50\%$, consistent with previous observations in Southern California and Duck, USA and the North Sea. The bound wave energy scaled with the local SS energy squared (with higher correlation to swell energy than sea) and depth dependence is consistent with h^{-5} scaling. Free IG energy scaled linearly with the local SS energy and with the tide level.

These dependencies were included in parameterization of the total (bound and free IG) shoreward propagating energy that depen on tide level and wave models or buoy observations of SS waves. Parameterization of the seaward propagating IG waves showed a similar tidal dependence, differing from Ardhuin et al. (2014). Using an observation-based frequency distribution for free IG energy, bound and free wave are included in synthetic IG timeseries used to initialize the nonlinear, phase-resolving, numerical wave model SWASH. SWASH results suggest that wave runup is weakly influenced by free shoreward propagating IG waves observed at the offshore boundary.

Further observations and modeling are needed to extent the present results to other coastal locations.

Open Research Section

The 2494 timeseries of pressure, cross-shore and alongshore velocity is available on Zenodo at `https://doi.org/10.5281/zenodo.8254388`.

Acknowledgments

This study was funded by the U.S. Army Corps of Engineers (W912HZ1920020) and the California Department of Parks and Recreation (C19E0026). Data were collected and processed by the Coastal Processes Group field team members Lucian Parry, Rob Grenzeback, Kent Smith, Brian Woodward, Greg Boyd, Shane Finnerty, Carson Black, and Mele Johnson. Michele Okihiro organized logistics.

References

Aagaard, T., & Greenwood, B. (1994, April). Suspended sediment transport and the role of infragravity waves in a barred surf zone. *Marine Geology*, *118*(1-2), 23–48. Retrieved 2023-04-27, from `https://linkinghub.elsevier.com/retrieve/pii/0025322794901112` doi: 10.1016/0025-3227(94)90111-2

Aagaard, T., & Greenwood, B. (2008, May). Infragravity wave contribution to surf zone sediment transport — The role of advection. *Marine Geology*, *251*(1-2), 1–14. Retrieved 2023-04-27, from `https://linkinghub.elsevier.com/retrieve/pii/S0025322708000297` doi: 10.1016/j.margeo.2008.01.017

Altomare, C., Bolle, A., Brand, E., Chen, M., Dan, S., De Sloover, L., … Zhange, Q. (2020). *CREST Final Scientific Report: Take Home Messages & Project Results.* VLIZ Special Publication 85.

Ardhuin, F., Devaux, E., & Pineau-Guillou, L. (2010). Observation et prévision des seiches sur la côte Atlantique française. In *XIèmes Journées, Les Sables d'Olonne* (pp. 1–8). Editions Paralia. Retrieved 2023-04-27, from `http://www.paralia.fr/jngcgc/11_01_ardhuin.pdf` doi: 10.5150/jngcgc.2010.001-A

Ardhuin, F., Rawat, A., & Aucan, J. (2014, May). A numerical model for free infragravity waves: Definition and validation at regional and global scales. *Ocean Modelling*, *77*, 20–32. Retrieved 2021-03-15, from `https://linkinghub.elsevier.com/retrieve/pii/S1463500314000274` doi: 10.1016/j.ocemod.2014.02.006

Baldock, T., Manoonvoravong, P., & Pham, K. S. (2010, October). Sediment transport and beach morphodynamics induced by free long waves, bound long waves and wave groups. *Coastal Engineering*, *57*(10), 898–916. Retrieved 2023-04-27, from `https://linkinghub.elsevier.com/retrieve/pii/S0378383910000694` doi: 10.1016/j.coastaleng.2010.05.006

Battjes, J. A. (2004). Shoaling of subharmonic gravity waves. *Journal of Geophysical Research*, *109*(C2), C02009. Retrieved 2019-05-13, from `http://doi.wiley.com/10.1029/2003JC001863` doi: 10.1029/2003JC001863

Behrens, J., Thomas, J., Terrill, E., & Jensen, R. (2019, March). CDIP: Maintaining a Robust and Reliable Ocean Observing Buoy Network. In

2019 IEEE/OES Twelfth Current, Waves and Turbulence Measurement (CWTM) (pp. 1–5). San Diego, CA, USA: IEEE. Retrieved 2023-04-06, from https://ieeexplore.ieee.org/document/8955166/ doi: 10.1109/CWTM43797.2019.8955166

de Bakker, A., Tissier, M., & Ruessink, B. (2014, January). Shoreline dissipation of infragravity waves. *Continental Shelf Research*, *72*, 73–82. Retrieved 2021-04-03, from https://linkinghub.elsevier.com/retrieve/pii/S0278434313003786 doi: 10.1016/j.csr.2013.11.013

De Bakker, A. T. M., Brinkkemper, J. A., Van Der Steen, F., Tissier, M. F. S., & Ruessink, B. G. (2016, October). Cross-shore sand transport by infragravity waves as a function of beach steepness: SAND TRANSPORT BY INFRAGRAVITY WAVES. *Journal of Geophysical Research: Earth Surface*, *121*(10), 1786–1799. Retrieved 2023-04-27, from http://doi.wiley.com/10.1002/2016JF003878 doi: 10.1002/2016JF003878

de Bakker, A. T. M., Herbers, T. H. C., Smit, P. B., Tissier, M. F. S., & Ruessink, B. G. (2015, February). Nonlinear Infragravity–Wave Interactions on a Gently Sloping Laboratory Beach. *Journal of Physical Oceanography*, *45*(2), 589–605. Retrieved 2021-04-03, from https://journals.ametsoc.org/view/journals/phoc/45/2/jpo-d-14-0186.1.xml doi: 10.1175/JPO-D-14-0186.1

Dusseljee, D., Klopman, G., Van Vledder, G., & Riezebos, H. J. (2014, December). IMPACT OF HARBOR NAVIGATION CHANNELS ON WAVES: A NUMERICAL MODELLING GUIDELINE. *Coastal Engineering Proceedings*, *1*(34), 58. Retrieved 2023-05-02, from https://journals.tdl.org/icce/index.php/icce/article/view/7710 doi: 10.9753/icce.v34.waves.58

Eckart, C. (1951). SURFACE WAVES ON WATER OF VARIABLE DEPTH.

Elgar, S., & Guza, R. T. (1985). Observations of bispectra of shoaling surface gravity waves. *Journal of Fluid Mechanics*.

Elgar, S., Herbers, T. H. C., & Guza, R. T. (1994, July). Reflection of Ocean Surface Gravity Waves from a Natural Beach. *Journal of Physical Oceanography*, *24*(7), 1503–1511. Retrieved 2023-04-30, from http://journals.ametsoc.org/doi/10.1175/1520-0485(1994)024<1503:ROOSGW>2.0.CO;2 doi: 10.1175/1520-0485(1994)024⟨1503:ROOSGW⟩2.0.CO;2

Elgar, S., Herbers, T. H. C., Okihiro, M., Oltman-Shay, J., & Guza, R. T. (1992). Observations of infragravity waves. , 5.

Elgar, S., Raubenheimer, B., & Guza, R. T. (2005, October). Quality control of acoustic Doppler velocimeter data in the surfzone. *Measurement Science and Technology*, *16*(10), 1889–1893. Retrieved 2023-04-11, from https://iopscience.iop.org/article/10.1088/0957-0233/16/10/002 doi: 10.1088/0957-0233/16/10/002

Fiedler, J. W., Smit, P. B., Brodie, K. L., McNinch, J., & Guza, R. (2018, January). Numerical modeling of wave runup on steep and mildly sloping natural beaches. *Coastal Engineering*, *131*, 106–113. Retrieved 2020-10-20, from https://linkinghub.elsevier.com/retrieve/pii/S037838391730193X doi: 10.1016/j.coastaleng.2017.09.004

Fiedler, J. W., Smit, P. B., Brodie, K. L., McNinch, J., & Guza, R. (2019, January). The offshore boundary condition in surf zone modeling. *Coastal Engineering*, *143*, 12–20. Retrieved 2019-08-14, from https://linkinghub.elsevier.com/retrieve/pii/S0378383918301984 doi: 10.1016/j.coastaleng.2018.10.014

Fiedler, J. W., Young, A. P., Ludka, B. C., O'Reilly, W. C., Henderson, C., Merrifield, M. A., & Guza, R. T. (2020, October). Predicting site-specific storm wave run-up. *Natural Hazards*, *104*(1), 493–517. Retrieved 2020-10-08, from http://link.springer.com/10.1007/s11069-020-04178-3 doi: 10.1007/s11069-020-04178-3

Gallagher, B. (1971, September). Generation of surf beat by non-linear wave interactions. *Journal of Fluid Mechanics*, *49*(1), 1–20. Retrieved 2021-03-01, from https://www.cambridge.org/core/product/identifier/S0022112071001897/type/journal_article doi: 10.1017/S0022112071001897

Guza, R. T., & Thornton, E. B. (1982). Swash oscillations on a natural beach. *Journal of Geophysical Research*, *87*(C1), 483. Retrieved 2020-06-08, from http://doi.wiley.com/10.1029/JC087iC01p00483 doi: 10.1029/JC087iC01p00483

Guza, R. T., & Thornton, E. B. (1985). Observations of surf beat. *Journal of Geophysical Research*, *90*(C2), 3161. Retrieved 2021-04-03, from http://doi.wiley.com/10.1029/JC090iC02p03161 doi: 10.1029/JC090iC02p03161

Hasselmann, K. (1962, April). On the non-linear energy transfer in a gravity-wave spectrum Part 1. General theory. *Journal of Fluid Mechanics*, *12*(04), 481. Retrieved 2020-10-08, from http://www.journals.cambridge.org/abstract_S0022112062000373 doi: 10.1017/S0022112062000373

Hasselmann, K., Munk, W. H., & MacDonald, G. (1963). *Bispectra of Ocean Waves.* Proc. of Time Series Analysis.

Henderson, C. S., Fiedler, J. W., Merrifield, M. A., Guza, R., & Young, A. P. (2022, August). Phase resolving runup and overtopping field validation of SWASH. *Coastal Engineering*, *175*, 104128. Retrieved 2023-04-06, from https://linkinghub.elsevier.com/retrieve/pii/S0378383922000436 doi: 10.1016/j.coastaleng.2022.104128

Henderson, S. M., Guza, R. T., Elgar, S., Herbers, T. H. C., & Bowen, A. J. (2006, December). Nonlinear generation and loss of infragravity wave energy. *Journal of Geophysical Research*, *111*(C12), C12007. Retrieved 2019-05-13, from http://doi.wiley.com/10.1029/2006JC003539 doi: 10.1029/2006JC003539

Herbers, T. H. C., Elgar, S., & Guza, R. T. (1995). Generation and propagation of infragravity waves. *Journal of Geophysical Research*, *100*(C12), 24863. Retrieved 2019-05-13, from http://doi.wiley.com/10.1029/95JC02680 doi: 10.1029/95JC02680

Herbers, T. H. C., Elgar, S., Guza, R. T., & O'Reilly, W. C. (1995). Infragravity-Frequency (0.005–0.05 Hz) Motions on the Shelf. Part II Free Waves. *Journal of Physical Oceanography*, 1063–1079.

Herbers, T. H. C., & Guza, R. T. (1994). Infragravity-Frequency (0.005–0.05 Hz) Motions on the Shelf. Part I Forced Waves. *Journal of Physical Oceanography*.

Huntley, D. A. (1976, December). Long-period waves on a natural beach. *Journal of Geophysical Research*, *81*(36), 6441–6449. Retrieved 2020-10-20, from http://doi.wiley.com/10.1029/JC081i036p06441 doi: 10.1029/JC081i036p06441

Huntley, D. A., Guza, R. T., & Thornton, E. B. (1981). Field observations of surf beat: 1. Progressive edge waves. *Journal of Geophysical Research*, *86*(C7), 6451. Retrieved 2021-03-02, from http://doi.wiley.com/10.1029/JC086iC07p06451 doi: 10.1029/JC086iC07p06451

Kim, Y. C., Beall, J. M., Powers, E. J., & Miksad, R. W. (1980). Bispectrum and nonlinear wave coupling. *Physics of Fluids*, *23*(2), 258. Retrieved 2019-06-01, from https://aip.scitation.org/doi/10.1063/1.862966 doi: 10.1063/1.862966

Kuik, A. (1988). *A Method for the Routine Analysis of Pitch-and-Roll Buoy Wave Data.* Journal of Physical Oceanography.

Lange, A. M., Fiedler, J. W., Becker, J. M., Merrifield, M. A., & Guza, R. (2022, March). Estimating runup with limited bathymetry. *Coastal Engineering*, *172*, 104055. Retrieved 2023-04-06, from https://linkinghub.elsevier.com/retrieve/pii/S0378383921001940 doi: 10.1016/j.coastaleng.2021.104055

Li, S., Liao, Z., Liu, Y., & Zou, Q. (2020, August). Evolution of Infragravity Waves Over a Shoal Under Nonbreaking Conditions. *Journal of Geophysical Research: Oceans*, *125*(8). Retrieved 2023-05-02, from https://onlinelibrary.wiley.com/doi/10.1029/2019JC015864 doi: 10.1029/2019JC015864

List, J. H. (1986). Wave Groupiness as a Source of Nearshore Long Waves. *COASTAL ENGINEERING*, 15.

Longuet-Higgins, M. S., & Stewart, R. W. (1962, August). Radiation stress and mass transport in gravity waves, with application to 'surf beats'. *Journal of Fluid Mechanics*, *13*(4), 481–504. Retrieved 2019-05-13, from `https://www.cambridge.org/core/product/identifier/S0022112062000877/type/journal_article` doi: 10.1017/S0022112062000877

Ludka, B. C., Guza, R. T., O'Reilly, W. C., Merrifield, M. A., Flick, R. E., Bak, A. S., ... Boyd, G. (2019, December). Sixteen years of bathymetry and waves at San Diego beaches. *Scientific Data*, *6*(1), 161. Retrieved 2020-07-27, from `http://www.nature.com/articles/s41597-019-0167-6` doi: 10.1038/s41597-019-0167-6

Mendes, D., Pinto, J. P., Pires-Silva, A. A., & Fortunato, A. B. (2018, October). Infragravity wave energy changes on a dissipative barred beach: A numerical study. *Coastal Engineering*, *140*, 136–146. Retrieved 2023-07-25, from `https://linkinghub.elsevier.com/retrieve/pii/S0378383918300322` doi: 10.1016/j.coastaleng.2018.07.005

Munk, W. H. (1949). Surf beats. *Transactions, American Geophysical Union*, *30*(6), 849. Retrieved 2019-05-28, from `http://doi.wiley.com/10.1029/TR030i006p00849` doi: 10.1029/TR030i006p00849

Nicolae Lerma, A., Pedreros, R., Robinet, A., & Sénéchal, N. (2017, May). Simulating wave setup and runup during storm conditions on a complex barred beach. *Coastal Engineering*, *123*, 29–41. Retrieved 2023-04-06, from `https://linkinghub.elsevier.com/retrieve/pii/S0378383916301284` doi: 10.1016/j.coastaleng.2017.01.011

Okihiro, M., & Guza, R. T. (1995). Infragravity energy modulation by tides. *Journal of Geophysical Research*, *100*(C8), 16143. Retrieved 2021-03-12, from `http://doi.wiley.com/10.1029/95JC01545` doi: 10.1029/95JC01545

Okihiro, M., Guza, R. T., & Seymour, R. J. (1992). Bound Infragravity Waves. *Journal of Geophysical Research*, *97*(C7), 11453–11469. Retrieved 2021-03-01, from `http://doi.wiley.com/10.1029/92JC00270` doi: 10.1029/92JC00270

Okihiro, M., Guza, R. T., & Seymour, R. J. (1993). Excitation of seiche observed in a small harbor. *Journal of Geophysical Research*, *98*(C10), 18201. Retrieved 2023-04-30, from `http://doi.wiley.com/10.1029/93JC01760` doi: 10.1029/93JC01760

Oltman-Shay, J., & Guza, R. T. (1987). *Infragravity Edge Wave Observations on Two California Beaches.pdf.* Journal of Physical Oceanography.

Oltman-Shay, J., & Howd, P. A. (1993, February). Edge waves on nonplanar bathymetry and alongshore currents: A model and data comparison. *Journal of Geophysical Research: Oceans*, *98*(C2), 2495–2507. Retrieved 2023-04-27, from `http://doi.wiley.com/10.1029/92JC02609` doi: 10.1029/92JC02609

O'Reilly, W., Olfe, C. B., Thomas, J., Seymour, R., & Guza, R. (2016, October). The California coastal wave monitoring and prediction system. *Coastal Engineering*, *116*, 118–132. Retrieved 2019-08-14, from `https://linkinghub.elsevier.com/retrieve/pii/S0378383916301120` doi: 10.1016/j.coastaleng.2016.06.005

Qin, L., & Li, Y. (2021, November). Significant Wave Height Estimation Using Multi-Satellite Observations from GNSS-R. *Remote Sensing*, *13*(23), 4806. Retrieved 2023-04-27, from `https://www.mdpi.com/2072-4292/13/23/4806` doi: 10.3390/rs13234806

Rawat, A., Ardhuin, F., Ballu, V., Crawford, W., Corela, C., & Aucan, J. (2014, November). Infragravity waves across the oceans: Following Infra-Gravity Wave Bursts. *Geophysical Research Letters*, *41*(22), 7957–7963. Retrieved 2021-04-02, from `http://doi.wiley.com/10.1002/2014GL061604` doi: 10.1002/2014GL061604

Reniers, A. J., Naporowski, R., Tissier, M. F. S., de Schipper, M. A., Akrish, G., & Rijnsdorp, D. P. (2021, January). North Sea Infragravity Wave Observations. *Journal of Marine Science and Engineering*, *9*(2), 141. Retrieved 2021-04-02, from `https://www.mdpi.com/2077-1312/9/2/141` doi: 10.3390/jmse9020141

Reniers, A. J. H. M. (2002). Linear modeling of infragravity waves during Delilah. *Journal of Geophysical Research*, *107*(C10), 3137. Retrieved 2021-04-02, from `http://doi.wiley.com/10.1029/2001JC001083` doi: 10.1029/2001JC001083

Rhie, J., & Romanowicz, B. (2006, October). A study of the relation between ocean storms and the Earth's hum: OCEAN STORMS AND EARTH'S HUM. *Geochemistry, Geophysics, Geosystems*, *7*(10), n/a–n/a. Retrieved 2023-04-27, from `http://doi.wiley.com/10.1029/2006GC001274` doi: 10.1029/2006GC001274

Ribal, A., & Young, I. R. (2019, May). 33 years of globally calibrated wave height and wind speed data based on altimeter observations. *Scientific Data*, *6*(1), 77. Retrieved 2023-04-27, from `https://www.nature.com/articles/s41597-019-0083-9` doi: 10.1038/s41597-019-0083-9

Rijnsdorp, D. P., Reniers, A. J. H. M., & Zijlema, M. (2021, August). Free Infragravity Waves in the North Sea. *Journal of Geophysical Research: Oceans*, *126*(8). Retrieved 2023-04-06, from `https://onlinelibrary.wiley.com/doi/10.1029/2021JC017368` doi: 10.1029/2021JC017368

Rijnsdorp, D. P., Ruessink, G., & Zijlema, M. (2015, June). Infragravity-wave dynamics in a barred coastal region, a numerical study. *Journal of Geophysical Research: Oceans*, *120*(6), 4068–4089. Retrieved 2021-04-02, from `https://onlinelibrary.wiley.com/doi/abs/10.1002/2014JC010450` doi: 10.1002/2014JC010450

Rijnsdorp, D. P., Smit, P. B., & Guza, R. (2022, August). A nonlinear, non-dispersive energy balance for surfzone waves: infragravity wave dynamics on a sloping beach. *Journal of Fluid Mechanics*, *944*, A45. Retrieved 2023-07-25, from `https://www.cambridge.org/core/product/identifier/S0022112022005122/type/journal_article` doi: 10.1017/jfm.2022.512

Rijnsdorp, D. P., Smit, P. B., & Zijlema, M. (2014, March). Non-hydrostatic modelling of infragravity waves under laboratory conditions. *Coastal Engineering*, *85*, 30–42. Retrieved 2023-05-02, from `https://linkinghub.elsevier.com/retrieve/pii/S0378383913001944` doi: 10.1016/j.coastaleng.2013.11.011

Roelvink, D., Reniers, A., Van Dongeren, A., Van Thiel De Vries, J., McCall, R., & Lescinski, J. (2009, November). Modelling storm impacts on beaches, dunes and barrier islands. *Coastal Engineering*, *56*(11-12), 1133–1152. Retrieved 2023-05-02, from `https://linkinghub.elsevier.com/retrieve/pii/S0378383909001252` doi: 10.1016/j.coastaleng.2009.08.006

Ruessink, B. G. (1998, June). Bound and free infragravity waves in the nearshore zone under breaking and nonbreaking conditions. *Journal of Geophysical Research: Oceans*, *103*(C6), 12795–12805. Retrieved 2019-05-13, from `http://doi.wiley.com/10.1029/98JC00893` doi: 10.1029/98JC00893

Ruessink, G., Michallet, H., Bonneton, P., Mouazé, D., Lara, J. L., Silva, P. A., & Wellens, P. (2013). GLOBEX: WAVE DYNAMICS ON A GENTLY SLOPING LABORATORY BEACH. *Coastal Dynamics*, 12.

Ruggiero, P. (2004). Wave run-up on a high-energy dissipative beach. *Journal of Geophysical Research*, *109*(C6), C06025. Retrieved 2021-03-12, from `http://doi.wiley.com/10.1029/2003JC002160` doi: 10.1029/2003JC002160

Ruju, A., Lara, J. L., & Losada, I. J. (2012, October). Radiation stress and low-frequency energy balance within the surf zone: A numerical approach. *Coastal Engineering*, *68*, 44–55. Retrieved 2023-04-30, from `https://linkinghub.elsevier.com/retrieve/pii/S0378383912000907` doi: 10.1016/j.coastaleng.2012.05.003

Ruju, A., Lara, J. L., & Losada, I. J. (2014, April). Numerical analysis of run-up oscillations under dissipative conditions. *Coastal Engineering*, *86*, 45–56. Retrieved 2020-10-08, from https://linkinghub.elsevier.com/retrieve/pii/S0378383914000192 doi: 10.1016/j.coastaleng.2014.01.010

Sand, S. E. (1982, January). Wave grouping described by bounded long waves. *Ocean Engineering*, *9*(6), 567–580. Retrieved 2021-03-01, from https://linkinghub.elsevier.com/retrieve/pii/0029801882900038 doi: 10.1016/0029-8018(82)90003-8

Sheremet, A., Guza, R. T., Elgar, S., & Herbers, T. H. C. (2002). Observations of nearshore infragravity waves: Seaward and shoreward propagating components. *Journal of Geophysical Research*, *107*(C8), 3095. Retrieved 2021-03-12, from http://doi.wiley.com/10.1029/2001JC000970 doi: 10.1029/2001JC000970

Smit, P. B., Janssen, T. T., Herbers, T. H. C., Taira, T., & Romanowicz, B. A. (2018, July). Infragravity Wave Radiation Across the Shelf Break. *Journal of Geophysical Research: Oceans*, *123*(7), 4483–4490. Retrieved 2023-04-30, from https://onlinelibrary.wiley.com/doi/10.1029/2018JC013986 doi: 10.1029/2018JC013986

Stockdon, H. F., Holman, R. A., Howd, P. A., & Sallenger, A. H. (2006, May). Empirical parameterization of setup, swash, and runup. *Coastal Engineering*, *53*(7), 573–588. Retrieved 2020-03-17, from https://linkinghub.elsevier.com/retrieve/pii/S0378383906000044 doi: 10.1016/j.coastaleng.2005.12.005

Suzuki, T., Altomare, C., Veale, W., Verwaest, T., Trouw, K., Troch, P., & Zijlema, M. (2017, April). Efficient and robust wave overtopping estimation for impermeable coastal structures in shallow foreshores using SWASH. *Coastal Engineering*, *122*, 108–123. Retrieved 2020-10-20, from https://linkinghub.elsevier.com/retrieve/pii/S0378383916302435 doi: 10.1016/j.coastaleng.2017.01.009

Thomson, J., Elgar, S., Raubenheimer, B., Herbers, T. H. C., & Guza, R. T. (2006). Tidal modulation of infragravity waves via nonlinear energy losses in the surfzone. *Geophysical Research Letters*, *33*(5), L05601. Retrieved 2019-05-16, from http://doi.wiley.com/10.1029/2005GL025514 doi: 10.1029/2005GL025514

Tucker, M. (1950, August). Surf beats: sea waves of 1 to 5 min. period. *Proceedings of the Royal Society of London. Series A. Mathematical and Physical Sciences*, *202*(1071), 565–573. Retrieved 2021-02-26, from https://royalsocietypublishing.org/doi/10.1098/rspa.1950.0120 doi: 10.1098/rspa.1950.0120

Valentini, N., Saponieri, A., Danisi, A., Pratola, L., & Damiani, L. (2019, September). Exploiting remote imagery in an embayed sandy beach for the validation of a runup model framework. *Estuarine, Coastal and Shelf Science*, *225*, 106244. Retrieved 2023-07-25, from https://linkinghub.elsevier.com/retrieve/pii/S0272771418310333 doi: 10.1016/j.ecss.2019.106244

van Dongeren, A., Battjes, J., Janssen, T., van Noorloos, J., Steenhauer, K., Steenbergen, G., & Reniers, A. (2007, February). Shoaling and shoreline dissipation of low-frequency waves. *Journal of Geophysical Research*, *112*(C2), C02011. Retrieved 2019-05-13, from http://doi.wiley.com/10.1029/2006JC003701 doi: 10.1029/2006JC003701

van Noorloos, J. C. (2003). Energy transfer between short wave groups and bound long waves on a plane slope.

Van Thiel De Vries, J., Van Gent, M., Walstra, D., & Reniers, A. (2008, December). Analysis of dune erosion processes in large-scale flume experiments. *Coastal Engineering*, *55*(12), 1028–1040. Retrieved 2023-05-02, from https://linkinghub.elsevier.com/retrieve/pii/S0378383908000860 doi: 10.1016/j.coastaleng.2008.04.004

Webb, S. C. (2007, February). The Earth's 'hum' is driven by ocean waves over the continental shelves. *Nature*, *445*(7129), 754–756. Retrieved 2023-04-30, from http://www.nature.com/articles/nature05536 doi: 10.1038/nature05536

Webb, S. C., Zhang, X., & Crawford, W. (1991). Infragravity waves in the deep ocean. , 14.

Zhang, Q., Toorman, E. A., & Monbaliu, J. (2020, June). Shoaling of bound infragravity waves on plane slopes for bichromatic wave conditions. *Coastal Engineering*, *158*, 103684. Retrieved 2023-05-02, from https://linkinghub.elsevier.com/retrieve/pii/S037838391930198X doi: 10.1016/j.coastaleng.2020.103684

Zheng, Z., Ma, X., Ma, Y., Huang, X., & Dong, G. (2021, December). Modeling of coastal infragravity waves using the spectral model WAVEWATCH . *Coastal Engineering*, *170*, 104016. Retrieved 2023-04-20, from https://linkinghub.elsevier.com/retrieve/pii/S0378383921001654 doi: 10.1016/j.coastaleng.2021.104016

Zijlema, M. (2012, October). MODELLING WAVE TRANSFORMATION ACROSS A FRINGING REEF USING SWASH. *Coastal Engineering Proceedings*, *1*(33), 26. Retrieved 2020-07-14, from https://icce-ojs-tamu.tdl.org/icce/index.php/icce/article/view/6479 doi: 10.9753/icce.v33.currents.26

Zijlema, M., Stelling, G., & Smit, P. (2011, October). SWASH: An operational public domain code for simulating wave fields and rapidly varied flows in coastal waters. *Coastal Engineering*, *58*(10), 992–1012. Retrieved 2020-10-08, from https://linkinghub.elsevier.com/retrieve/pii/S0378383911000974 doi: 10.1016/j.coastaleng.2011.05.015

Free infragravity waves on the inner shelf: Observations and Parameterizations at two Southern California beaches

A.M.Z. Lange[1], J.W. Fiedler[1], M.A. Merrifield [1], and R.T. Guza[1]

[1]Scripps Institution of Oceanography, La Jolla, CA, USA

Key Points:

- Infragravity (IG) waves on the inner shelf (10-15m depth) in San Diego, USA are usually dominated by refractively trapped free waves.
- Seaward and shoreward propagating free IG energies are parameterized as a function of tide level and local sea-swell conditions.
- On a low slope (0.02) beach, numerical modeled wave runup is weakly influenced by the shoreward IG waves observed at the offshore boundary.

Corresponding author: Athina M.Z. Lange, `alange@ucsd.edu`

Abstract

Co-located pressure and velocity observations in 10-15m depth are used to estimate the relative contribution of bound and free infragravity (IG) wave energy to the IG wave field. Shoreward and seaward going IG waves are analyzed separately. At the Southern California sites, shoreward propagating IG waves are dominated by free waves, with the bound wave energy fraction $< 30\%$ for moderate energy incident sea-swell and $< 10\%$ for low energy incident sea-swell. Only the 5% of records with energetic long swell show primarily bound waves. Consistent with bound IG wave theory, the energy scales as the square (frequency integrated) sea-swell energy, with a higher correlation with swell than sea energy. Seaward and shoreward free IG energy is strongly tidally modulated. The ratio of free seaward to shoreward propagating IG energy suggests between 50-100% of the energy radiated offshore is trapped on the shelf seaward of 10-15m and redirected shoreward. Remote sources of IG energy are small. The observed linear dependency of free seaward and shoreward IG energy on local sea-swell wave energy and tide are parameterized with good skill ($R^2 \sim 0.90$). Free (random phase) and bound (phase-coupled) IG waves are included in numerically simulated timeseries for shoreward IG waves that are used to initialize ($\sim$ 10m depth) the numerical nonlinear wave transformation SWASH. On the low slope study beach, wave runup is only weakly influenced by free shoreward propagating waves observed at the offshore boundary (foreshore slope = 0.02).

Plain Language Summary

Infragravity (IG) waves are long-period (every 25 sec to 2.5 min) waves that contribute to coastal flooding and beach erosion. IG waves, generated near the shoreline by short-period sea-swell (SS) wave groups (known by surfers as “sets”), have long wavelengths (100s of m) and do not curl and break like ordinary sea and swell waves. Instead, they can bounce off the beach face and propagate seaward. Our study concerns IG waves on the inner shelf ($10 - 15$m depth, $\sim 500 - 700$m offshore), seaward of the region of IG generation. Similar to previous observations in Hawai'i and North Carolina, we find most of the bounced, seaward going IG energy cannot reach deep water and is trapped on the continental shelf. We develop an observation-based estimate IG wave energy on the inner shelf as a function of SS wave energy and tide level. Finally. we show with a numerical model that IG wave runup at the shoreline is influenced only weakly by IG waves on the inner shelf.

1 Introduction

Infragravity (IG) waves are low-frequency surface-gravity ocean waves with periods typically between 25-200s, longer period than the sea-swell waves that generate them. IG waves were first observed (Munk, 1949; Tucker, 1950) seaward of the surfzone, traveling shoreward with the group velocity of short-period wind-generated waves and $\sim 10\%$ of their amplitude. IG waves can contribute significantly to runup (Huntley, 1976; Guza & Thornton, 1982; Ruggiero, 2004; Stockdon et al., 2006, and many others), sediment transport (Aagaard & Greenwood, 1994, 2008; Baldock et al., 2010; De Bakker et al., 2016), harbor seiches (Okihiro et al., 1993; Ardhuin et al., 2010) and earth hum (Rhie & Romanowicz, 2006; Webb, 2007).

Shoaling, shoreward propagating sea-swell (SS) frequencies interact and transfer energy to their sum (higher-order harmonics) and difference (infragravity) frequencies through nonlinear triad interactions (Hasselmann et al., 1963; Elgar & Guza, 1985; van Dongeren et al., 2007). 'Bound waves' are shoreward propagating IG waves that are 180° out of phase with the envelope of higher-frequency sea-swell waves (Longuet-Higgins & Stewart, 1962). As shoaling SS waves become increasingly nondispersive, the bound wave approaches resonance, lags behind the wave group, and is eventually a ‘free’ wave (on the dispersion curve) that propagates to shore (List, 1986; Battjes, 2004; A. T. M. de

Bakker et al., 2015). Throughout the short wave (e.g. sea-swell) surf zone, free shoaling IG waves can acquire and lose energy from SS waves and can potentially break. At the shoreline, free IG waves can reflect and propagate seaward (Battjes, 2004; Thomson et al., 2006; S. M. Henderson et al., 2006; van Dongeren et al., 2007; Ruju et al., 2012; A. de Bakker et al., 2014).

In many locations, incident SS waves are relatively well characterized with buoys (Behrens et al., 2019), satellites (Ribal & Young, 2019; Qin & Li, 2021), and regional or global (e.g. WAVEWATCH III) wave models. While these SS waves can be used in offshore boundary conditions (BC) for surf zone models, typically in $\sim 10-20$m depth, the contribution of IG waves is not accurately observed or predicted by these systems. IG waves, typically observed with bottom-mounted pressure and/or current sensors, are less widely observed and characterized (Okihiro et al., 1992; Ardhuin et al., 2014; A. J. Reniers et al., 2021). The practical limitations of direct observations of infragravity waves motivates the present efforts to parameterize IG energy for use in nearshore models. Bound wave theory has been implemented as an offshore IG boundary condition in laboratory studies where the wavemaker is carefully controlled to create only a shoreward propagating bound IG wave and (ideally) to absorb seaward propagating IG waves (van Noorloos, 2003; Van Thiel De Vries et al., 2008; G. Ruessink et al., 2013; Altomare et al., 2020, and resulting papers). The offshore boundary condition in field settings have included theoretical bound waves and also observed timeseries (Roelvink et al., 2009; Zijlema, 2012; A. de Bakker et al., 2014; A. T. M. de Bakker et al., 2015; Dusseljee et al., 2014; Rijnsdorp et al., 2014, 2015; Fiedler et al., 2019; Zhang et al., 2020; Li et al., 2020; C. S. Henderson et al., 2022). The effect of free shoreward propagating IG waves in the model offshore boundary has received little attention, and no existing parameterization includes both 2D bound and free IG waves. Here, 3 years of pressure and current (PUV) data in 10-15m depth are used to determine (and parameterize) the variation of incident IG waves with a range of SS waves. A parametric offshore IG boundary condition is developed.

1.1 Bound Waves

Bound infragravity spectral energy $E_{IG}^{bound} = \int_{IG} \mathbf{E}^{bound}(f)df$ is estimated from second-order nonlinear wave theory (Hasselmann, 1962; Sand, 1982; Herbers, Elgar, & Guza, 1995, and many others).

$$\mathbf{E}_{IG}^{bound}(\Delta f, \Delta\theta) = 2 \int_{\Delta f} D^2 S(f, \theta_1) S(f + \Delta f, \theta_2) df, \tag{1}$$

$$\begin{aligned} D = &\quad \frac{-gk_1k_2\cos(\Delta\theta)}{2\omega_1\omega_2} + \frac{1}{2g}(\omega_1^2 + \omega_2^2 + \omega_1\omega_2) + C\frac{g(\omega_1+\omega_2)}{(gk_3\tanh(k_3h) - (\omega_1+\omega_2)^2) * \omega_1\omega_2}, \\ C = &\quad (\omega_1 + \omega_2) * \left(\frac{\omega_1\omega_2}{g}\right)^2 - k_1k_2\cos(\Delta\theta) - \frac{1}{2}\left(\frac{\omega_1 k_2^2}{\cosh^2(k_2h)} + \frac{\omega_2 k_1^2}{\cosh^2(k_1h)}\right), \end{aligned}$$

with wavenumber k, angular frequency ω $(= 2\pi f)$ and where the sea-swell frequency-direction spectra $S(f, \theta)$ can be estimated from a PUV, a pitch-roll buoy (Kuik, 1988), or a regional wave model. The interaction coefficient D is computed for the difference frequency (Δf) of every frequency pair (f_1, f_2) and if assuming directionally spread waves (2D), every difference direction $(\Delta\theta = \theta_2 - \theta_1 + 180°)$. D varies strongly as a function of $\Delta\theta$, depth, and SS frequency f. In shallow water, D is maximum (D_{max}) for co-linear $(\Delta\theta = 0)$ waves, and 1D theory $(\Delta\theta = 0)$ is the upper limit on bound wave energy. D decreases quickly with increasing $\Delta\theta$; $\Delta\theta = 30°$ results in $D \sim 25\% D_{max}$ (Herbers & Guza, 1994). The theoretical sensitivity of 2D bound wave energy to $S(f, \theta)$ and the fundamentally low resolution of a single PUV directional estimator limits the accuracy of the present 2D bound wave estimates. The coupling coefficient is frequency dependent and swell $(8-25\text{s})$ produces larger bound waves than sea $(4-8\text{s})$ (Okihiro et al., 1992).

Bound IG waves can alternatively be estimated with the third-order spectrum (bispectrum, Hasselmann et al., 1963; Kim et al., 1980; Elgar & Guza, 1985) that depends on nonlinear phase coupling between wave triads with angular frequencies ω_1, ω_2, ω_{1+2}. The bispectrum is the expected value of the triple product of complex Fourier coefficients, $B(k,l) = \tilde{E}[X_k X_l X_{k+l}]$.

With random phases and no nonlinear coupling of the three frequencies, the bispectrum vanishes. The normalized magnitude of the bispectra ($\mathbf{b}$, bicoherence),

$$\mathbf{b}(f_1, f_2) = \frac{B(f_1, f_2)}{\sqrt{\mathbf{E}(f_1)\mathbf{E}(f_2)\mathbf{E}(f_1 + f_2)}}, \tag{2}$$

measures the strength of the phase coupling between the three waves. The bispectrum phase (biphase) corresponds to the phase lag between the IG wave and the SS wave group (Elgar & Guza, 1985). The forced wave spectral density is the bispectrum integrated over all frequency pairs for a given difference frequency (Herbers & Guza, 1994),

$$\mathbf{E}_{IG}^{forced}(\Delta f) = \alpha(\Delta f)|b_i(\Delta f)|^2 \mathbf{E}(\Delta f), \tag{3}$$

$$\mathbf{b}_i(\Delta f) = 2\int_{\Delta f}^{\inf} df B(f, \Delta f) / \sqrt{2\int_{\Delta f}^{\inf} df \mathbf{E}(f + \Delta f)\mathbf{E}(f)\mathbf{E}(\Delta_f)}, \tag{4}$$

and the bias term α can be computed from the bound wave theory.

1.2 Free Waves

Free waves contribute significantly to IG waves (Gallagher, 1971; Huntley et al., 1981; Oltman-Shay & Guza, 1987; Okihiro et al., 1992; Zijlema, 2012; Smit et al., 2018). 'Edge' waves are free waves trapped on a sloping beach by shoreline reflection and back-refraction by the increasing water depth (Eckart, 1951). Edge waves are sensitive to geography, with the amount of trapping depending on the continental shelf and beach topography (Herbers, Elgar, Guza, & O'Reilly, 1995). Seaward propagating IG waves that propagate freely from the shoreline across the shelf to deep water are known as 'leaky' waves (Webb et al., 1991; Ardhuin et al., 2014; Rijnsdorp et al., 2021). Ardhuin et al. (2014) and Rawat et al. (2014) parameterize seaward-going free wave energy (radiated from the surfzone) for use as an incident boundary condition for global model WAVEWATCH III, but the free IG wave climate on the inner shelf is poorly understood.

Previous work in Duck, NC, Southern California, and Hawai'i, USA and the North Sea have investigated the fraction of IG energy contained in the bound component, giving an indication of the amount of free shoreward wave energy. Numerous studies at Duck, NC ($\sim$ 8−13m depth) (Elgar et al., 1992; Herbers & Guza, 1994; B. G. Ruessink, 1998; A. J. H. M. Reniers, 2002) found that the bound wave fraction was typically between 10−20%, with higher values above 30% (and up to 100%) only during the most energetic SS conditions. In the North Sea ($\sim$ 30m depth), IG wave conditions are always free wave dominant and only during the peak of storms is the fraction bound $\geq$ 50% (A. J. Reniers et al., 2021). At beaches in Southern California and Hawai'i ($\sim$ 8−13m and 183m depth) (Okihiro et al., 1992), up to 50% of the IG energy is at times attributed to bound wave energy. The bound fraction is dependent on water depth; Elgar et al. (1992) observed twice the bound fraction in 8m depth compared to 13m depth in Duck, NC. Torrey Pines has long been a study site for refractively trapped waves (Huntley et al., 1981; Guza & Thornton, 1985; Oltman-Shay & Guza, 1987; Oltman-Shay & Howd, 1993; Thomson et al., 2006), with significant trapped IG energy detected shoreward of 15m water depth. This refracted energy then propagates onshore as free waves. These trapped waves are not phase-coupled to local (instantaneous) SS wave groups because they are not generated locally in space or time.

In this study, we analyze the relative contribution of bound and free IG energy to the total IG energy in $10-15$m water depth for beaches in San Diego County, USA, confirm theoretical estimates of the incident bound wave energy, investigate parameterizations for both bound and free IG energy and estimate an IG sea surface elevation time-series that can be used as an incident boundary condition for nearshore models. Section 2.1 describes the dataset and quality control. Section 2.2 confirms that directional bound wave theory (Hasselmann, 1962) accurately predicts the observed bound wave energy. In Section 2.2 and 2.3, the relative contributions of shoreward propagating bound and free IG waves and their respective dependencies on the SS wave field are presented and compared with previous observations from other sites. The total incident bound and free IG energy and the spectral shape of the free energy are discussed in Section 3. Comparison to a previously developed seaward IG parameterization (Ardhuin et al., 2014), the tidal dependence and the effect of the IG BC in a phase-resolving nearshore numerical model on IG swash is presented in Section 4.

2 Observations

2.1 Data

Bottom-mounted pressure sensors and current meters (PUV) were deployed in 10 and 15-m depths at Torrey Pines State Beach and Cardiff State Beach, CA intermittently between Fall 2019 and Spring 2022 (Figure 1 and Table 1). Data were collected continuously between Fall 2021 and Spring 2022 as part of the Runup and Bathymetry 2D (RuBy2D) experiment at Torrey Pines, a 3km long, alongshore-uniform composite (summer sand, winter cobbles) beach. Cardiff is a 1.8km alongshore-variable beach, with a rocky reef beginning approximately 125m offshore at the southern end (Ludka et al., 2019). The 2 Hz PUV data were segmented into 3h records. The three largest tidal constituents are removed from the bottom pressure and velocity records, and the records are surface-corrected using linear finite-depth theory over the frequency band $0.004-0.25$ Hz. Computed spectra are segmented in 7200s demeaned ensembles, with an applied 50% overlapping Hanning window, with 0.0003 Hz frequency resolution and 13 degrees of freedom. The IG band is defined between $0.004-0.04$ Hz, the swell band between $0.04-0.12$ Hz and the sea band between $0.12-0.25$ Hz. As quality control, 3-hour pressure and velocity spectra passed a Z-test (Eq. 1 in Elgar et al., 2005),

$$Z^2 = \frac{P^2}{\left(\frac{\omega}{gk}\right)^2 \frac{\cosh^2 kh_P}{\cosh^2 kh_U}(U^2+V^2)}, \tag{5}$$

with cutoffs of $0.8 < Z_{IG} < 1.2$ and $0.95 < Z_{SS} < 1.05$. This confirms the use of linear theory in the sea surface correction. Additionally, only records with reflection coefficients (Eq. 4 in Sheremet et al., 2002) of $\mathscr{R}^2_{SS} < 0.25$ and $\mathscr{R}^2_{IG} < 2.5$ are used further. Only 5 values are removed with $\mathscr{R}^2_{IG} > 2.5$ with max $\mathscr{R}^2_{IG} = 2.9$. Details of the resulting 2494 quality controlled 3h records and SS bulk wave statistics are in Table 1. Spectral wave model (MOPS, O'Reilly et al., 2016) hindcast data from the observation periods show similar distributions of bulk parameters as a 23-year hindcast (Figure 2). The present observations are representative of the San Diego wave climate. Sea-surface elevation and velocity are combined to estimate shoreward and seaward propagating wave components, following Sheremet et al. (2002). Unless explicitly stated, the shoreward sea-surface elevation timeseries is used below to characterize the offshore boundary condition for wave propagation models.

2.2 Bound Waves

The 1D and 2D ($\pm 90°$ from shorenormal directionally-integrated) bound wave energies (Hasselmann, 1962) show the effects of directional spreading on the interaction

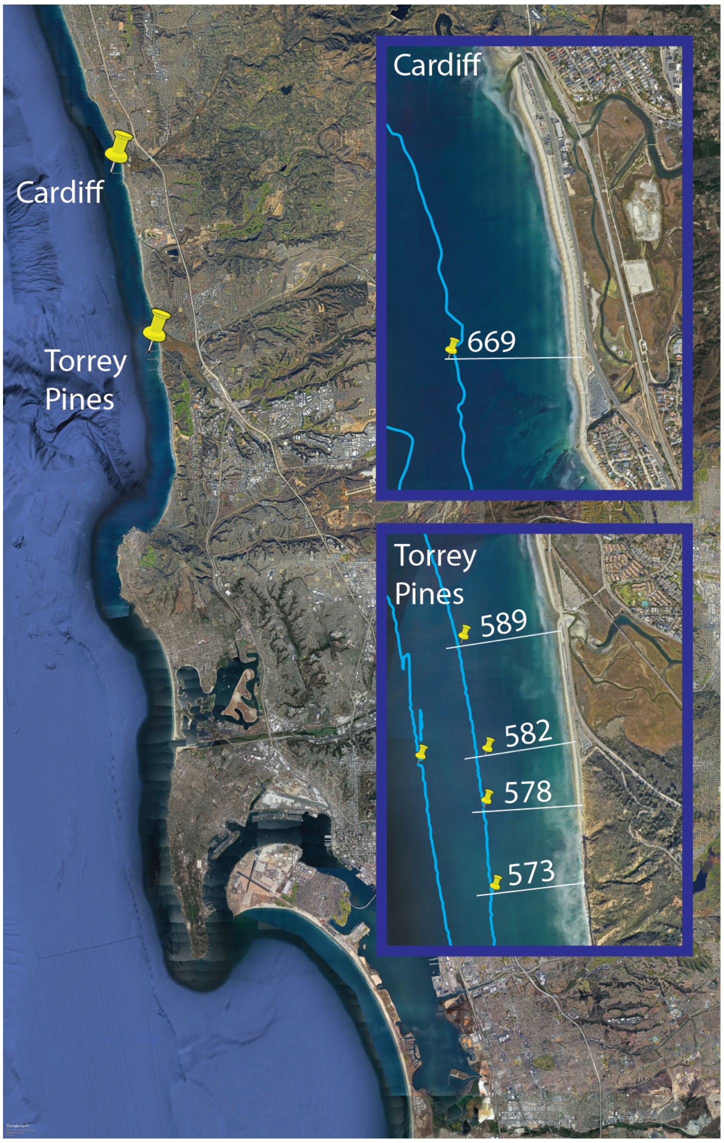

Figure 1. Co-located near-bottom pressure and biaxial acoustic current meter (PUV) in 10m and 15m depth at Torrey Pines and 10m depth at Cardiff. The Scripps Institution of Oceanography's wave MOnitoring and Prediction (MOP) (O'Reilly et al., 2016) transect numbers are given along with the 10 and 15m depth contours (NAVD88m).

coefficient D (Eq. 1 and Figure 3). The 1D estimates are about $\sim$ 3x larger than the directionally-integrated 2D estimates.

Bispectral analysis confirms 2D nonlinear theory (Hasselmann, 1962)(Figure 4). However, bispectral E_{IG}^{forced} estimates can be inaccurate when nonlinear coupling is weak, bound wave energy is low and free waves dominate. At individual frequencies, the bispectral and the bound wave estimates can differ by as much as a factor of 50 (Figure 3 and Herbers and Guza (1994)). Integrated over IG frequencies, the 2D bound wave and the forced wave energy (for fraction bound $> 15\%$) agree well ($R^2 = XX$, Figure 4). The cases of fraction bound $> 15\%$ are typically larger SS events (back-refracted deep water wave height H_0 and wavelength L_0 give median $\sqrt{H_0 L_0} = 13.1$m, compared to

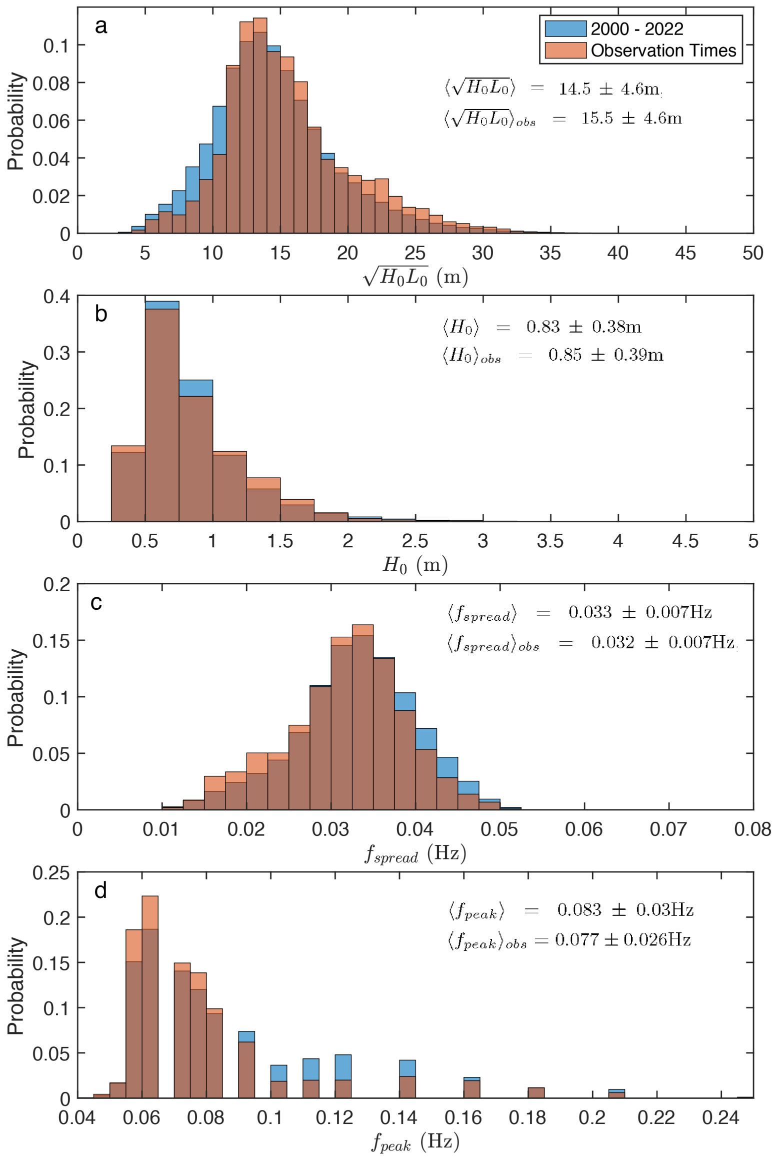

Figure 2. Histograms of (a) Offshore wave height H_0 and offshore wavelength L_0 in $\sqrt{H_0L_0}$, (b) H_0, (c) frequency spread f_{spread}, and (d) peak frequency f_{peak} at Torrey Pines in 10m at MOP582. Histograms are similar for 2000 - 2022 hindcast (blue, 201,600 1h values) and present observations (orange, 12,602 1h records). Mean $\pm$ 1 standard deviation of the full 23 year hindcast and over the present observation time period (MOPS) are given.

MOP	Date	Depth (m)	Distance from backbeach (m)	# of records	H_{SS} (m)	T_p (s)	D_p (degrees)	D_{spread} (degrees)
582	11/19 - 04/20	10	580	316	0.3 - 2.4	5 - 21	0 - 23	7 - 21
582	10/20 - 03/21	10	580	315	0.3 - 4.1	5 - 21	0 - 25	9 - 22
582	07/21 - 09/21	10	580	223	0.4 - 1	5 - 19	0 - 29	14 - 24
669	07/21 - 09/21	10	600	285	0.4 - 1.1	5 - 20	1 - 32	6 - 25
573	10/21 - 03/22	10	600	281	0.4 - 2.5	5 - 19	0 - 28	8 - 22
578	10/21 - 11/21	10	630	55	0.4 - 1.7	9 - 20	1 - 10	10 - 22
582	10/21 - 02/22	10	630	323	0.3 - 2.3	5 - 20	0 - 19	9 - 21
582	10/21 - 02/22	15	1020	401	0.5 - 2.7	5 - 20	0 - 25	8 - 25
589	10/21 - 02/22	10	660	289	0.3 - 2.3	6 - 20	0 - 32	9 - 22

Table 1. PUV Bulk Statistics. MOP location (580s are Torrey Pines and 669 is Cardiff in O'Reilly et al. (2016); Ludka et al. (2019)), date range, depth, distance from backbeach to PUV, the number of records for each PUV, significant wave height H_{SS}, peak period T_p, peak direction D_p and spread D_{spread}.

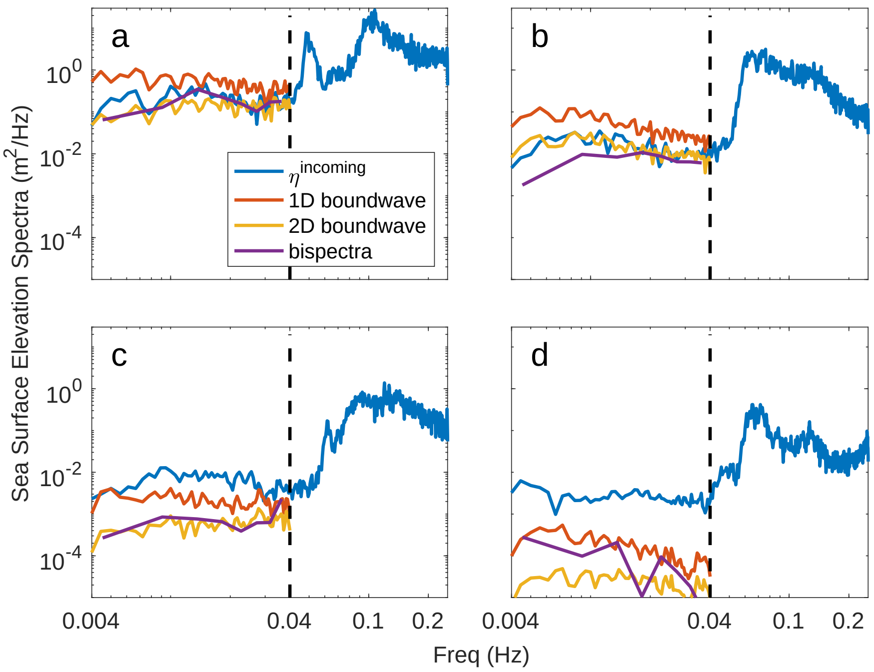

Figure 3. Observed (blue) sea surface elevation frequency spectra $\mathbf{E}(f)$ (d.o.f. = 30) in 10m for varying sea-swell wave heights H_{SS} (a) H_{SS} = 3.7m, $D_{spread,SS}$ = 18°, fraction bound = 74% (b) H_{SS} = 1.4m, $D_{spread,SS}$ = 13°, fraction bound = 100%, (c) H_{SS} = 1.0m, $D_{spread,SS}$ = 17°, fraction bound = 10%, and (d) H_{SS} = 0.4m, spread $D_{spread,SS}$ = 24°, fraction bound = 1%. In the IG band (f < 0.04 Hz, dashed vertical line), theoretical results are shown for 1D bound wave and 2 D bound wave, and for a bispectral approach (Herbers & Guza, 1994). Fraction bound (based on 2D bound waves) ranges from about 100% (a, largest H_{SS}) to 1% (d, smallest H_{SS}).

the median of the dataset = 10.7m). Analysis below uses 2D bound wave theory that (unlike bispectral estimates) does not rely on insitu IG observations and can be estimated from SS spectral waves from a buoy or wave model. Only 5% of the cases (120/2488) have a fraction bound greater than 50% (Figure 5 d). Similar to previous observations (Herbers, Elgar, & Guza, 1995; B. G. Ruessink, 1998) the fraction bound increases with increasing E_{IG} and E_{SS} and decreasing depth (or tide stage) (Figure 5 a). The frequency dependence of the bound wave coupling coefficient is seen with E_{IG}^{bound} being more highly correlated with E_{swell} ($R^2 = 0.84$) than E_{sea} ($R^2 = 0.59$) (Okihiro et al., 1992; Elgar et al., 1992).

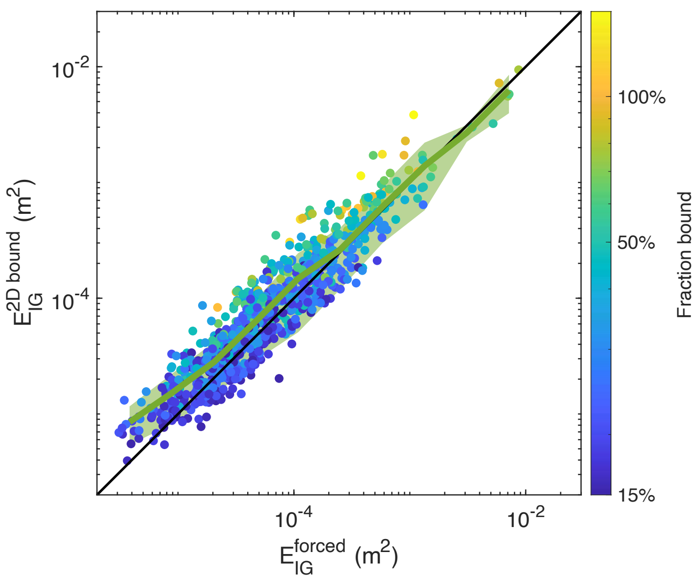

Figure 4. Bound IG energy from nonlinear 2D theory (Hasselmann, 1962) versus an estimate E_{IG}^{forced} based on bispectral analysis (Herbers & Guza, 1994). Colors are fraction bound based on 2D bound wave theory. When fraction bound < 15% bispectral results are widely scattered, and not shown or included in R^2. The 1-1 line, and mean and standard deviation for binned data (green curve and shading) are shown.

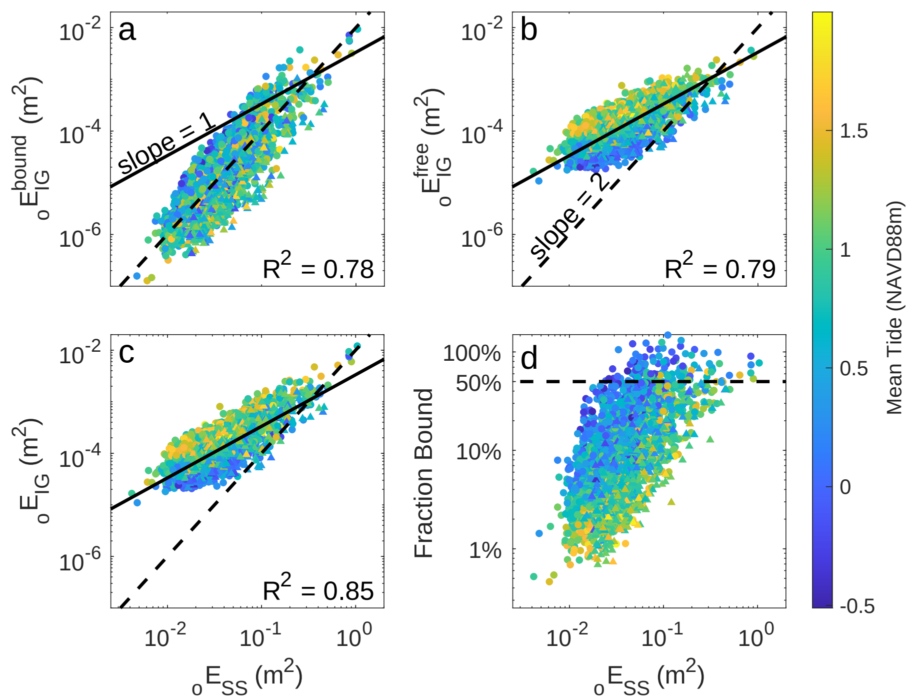

Figure 5. Observed shoreward propagating IG energy (a)E_{IG}^{bound}, (b) E_{IG}^{free}, (c) E_{IG}^{total}, and (d) fraction bound versus E_{SS}. Most observed fraction bound are < 50% (dashed horizontal line) and many are < 10%. △ is 15m PUV data. Correlations R^2 are given. E_{IG}^{bound} scales as E_{SS}^2 whereas both total and free IG energy scale as E_{SS}. In panels (a - c), the solid line shows a linear dependence on E_{SS} (slope = 1), and dashed line shows a quadratic dependence on E_{SS} (slope = 2).

2.3 Free Waves

The shoreward free IG energy spectra are estimated by subtracting the bound wave estimate ($\mathbf{E}_{IG}^{bound}(f)$) from the total shoreward IG energy spectra. These shoreward-directed free waves are a combination of refractively trapped (and typically locally generated) waves and leaky waves from remote sources. The free (and due to the dominance of free wave IG energy, the total) wave energy is approximately linearly proportional to E_{SS} (Figure 5 b, c, and consistent with Herbers, Elgar, Guza, & O'Reilly, 1995; Okihiro & Guza, 1995). This linear dependence on E_{SS}, as opposed to a quadratic dependence for the bound wave, has been attributed to dissipation (Herbers, Elgar, Guza, & O'Reilly, 1995). Free waves have a weaker depth dependence (h^{-1}) than bound waves (h^{-5}), consistent with Herbers, Elgar, Guza, and O'Reilly (1995).

Okihiro et al. (1992) estimated that in Southern California for typical SS energy, 25% of the IG energy was bound in 8-13m depth, 70% was trapped shoreward of a sensor in 183m depth, and only 5% was leaky. Leaky, free IG waves can propagate across ocean basins and in deep water appear uncoupled from and uncorrelated with local SS wave conditions (Webb et al., 1991; Ardhuin et al., 2014). However, on the inner shelf, remotely generated IG waves only dominate local IG waves when E_{SS} is very low (Herbers, Elgar, Guza, & O'Reilly, 1995; Sheremet et al., 2002). Remotely generated IG waves (i.e., unrelated to local SS wave energy) are not considered in the following analysis and contribute to parameterization noise.

3 Parameterizing the IG wave field

3.1 Bound Waves

Although 2D bound wave energy can be determined from the incident sea-swell spectrum, parameterizations of the total bound wave energy from bulk sea-swell wave statistics are convenient. Linear regression between ${}_{pred}E_{IG}^{bound}$ and $E_{SS}^2 h^{-5}$ (with exponents predicted in Herbers, Elgar, and Guza (1995) and similar to B. G. Ruessink (1998)), yields correlation coefficients R^2 between 0.58−0.91, for 10m Torrey Pines, 15m Torrey Pines and 10m Cardiff PUVs. A frequency-weighted sea-swell energy integral $\left(\int_{SS}\mathbf{E}(f)f^{-1}df\right)$ (similar to the approach of Fiedler et al. (2020)) has higher correlations in all cases (Eq. 6 with $R^2 = 0.84 - 0.97$, 95% CI $[14.98, 15.37]$, Figure 6 a),

$$
{}_{p}E_{IG}^{bound} = 15.2\left(\int_{SS}\mathbf{E}(f)f^{-1}df\right)^2 h^{-5}. \tag{6}
$$

The units of the dimensional constant on the right-hand side are selected to yield m^2.

3.2 Shoreward Free Waves

Linear regression between ${}_{obs}E_{IG}^{free}$ and E_{SS} gives correlation $R^2 = 0.79$ (Figure 5). However, similar to the bound wave parameterization, a frequency-weighted SS energy integral increases the correlation ($R^2 = 0.84$). The observed tidal dependence of free IG energy is accounted for with the normalized tide

$$
\tilde{\sigma} = \frac{\text{tide}_{obs} - \text{tide}_{low}}{\text{tide}_{high} - \text{tide}_{low}}, \tag{7}
$$

where 2.5m is the total tidal range observed across all deployments), with $\tilde{\sigma} = 0$ at the lowest observed tide (−0.5 NAVD88m), and $\tilde{\sigma} = 1$ at the highest tide (2 NAVD88m). Tide data is the 3h average obtained from a NOAA tide gauge (Station 9410230, La Jolla). Including a linear $\tilde{\sigma}$ dependence in the regression improves the correlation between observed and predicted total E_{IG}^{free} energy to $R^2 = 0.9$ (95% CI $[0.00066, 0.00068]$, Eq. 8, Figure 6 b) at all but the lowest tides and E_{SS},

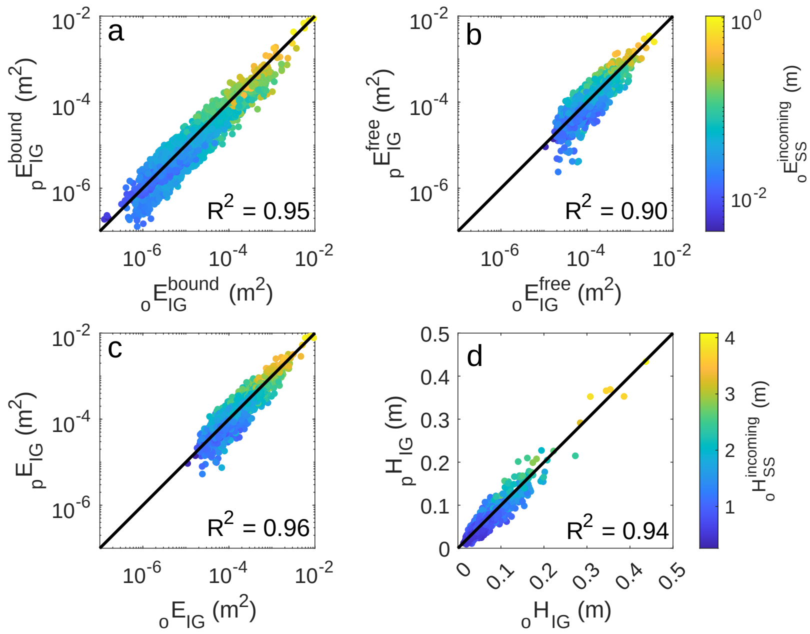

Figure 6. Parameterizations of incident IG wave field. (a) 2D bound wave parameterization (Eq. 6), (b) Free wave parameterization (Eq. 8), (c) 2D bound wave theory + free wave parameterization, colored by total incident SS energy (see color bar in (b)) and (d) significant wave height of estimated IG timeseries, colored by SS significant wave height.

	$\int_{SS} \mathbf{E}(f)df$	$\int_{SS} \mathbf{E}(f)f^{-1}df$	$\tilde{\sigma} \int_{SS} \mathbf{E}(f)f^{-1}df$
10m Torrey Pines	0.82	0.88	0.92
15m Torrey Pines	0.63	0.74	0.84
10m Cardiff	0.5	0.69	0.87
Total	0.79	0.84	0.9

Table 2. R^2 between total (frequency-band integrated) free shoreward IG energy observed and three parameterizations using the observed sea-swell wave energy spectrum $\mathbf{E}_{SS}(f)$. PUV sensors were deployed in 10m and 15m at Torrey Pines and 10m at Cardiff (see Table 1 for details). In all cases, $\tilde{\sigma} \int_{SS} \mathbf{E}(f)f^{-1}df$ has the highest R^2, where $\tilde{\sigma}$ is the relative tide level (Eq. 7).

$$ {}_pE_{IG}^{free} = 0.00067\tilde{\sigma} \int_{SS} \mathbf{E}(f)f^{-1}df. \tag{8} $$

Correlations in different depths and beaches are given in Table 3.2.

The total shoreward IG energy, with contributions from both bound and free waves can be estimated with local SS parameters. The parameterization performs well ($R^2 =$ 0.96) for all but the smallest E_{SS} and/or tides using either the bound wave parameterization (Eq. 6) or the integrated 2D Hasselmann bound wave energy (Figure 6 c). With the smallest E_{SS} and lowest tides, the parameterization underpredicts E_{IG} perhaps owing to free waves from remote sources (Webb et al., 1991; Ardhuin et al., 2014) and the inaccuracy of Eq. 6) when $\tilde{\sigma} = 0$.

Functional forms of the frequency distribution of the free IG energy were compared with the observed free IG spectra (normalized by the frequency-weighted SS energy). Forms investigated include linear and cubic fits to the median spectral shape, the spectral shape of Ardhuin et al. (2014) and an altered form (referred to as *nouvelleArdhuin*, Eq. 9),

$$A(f) = \begin{cases} \beta \frac{1}{\Delta f} * [f/0.012\text{Hz}] & \text{when } f < 0.012\text{Hz} \\ \beta \frac{1}{\Delta f} * [0.012\text{Hz}/f] & \text{when } f > 0.012\text{Hz} \end{cases}, \tag{9}$$

with $\beta = 0.0146$ (median spectral energy density at $f = 0.012$Hz).

NouvelleArdhuin has the smallest (~ 0.35) median root-mean-square logarithmic error (RMSLE) between ${}_{obs}E_{IG}^{free} * A(f)$ and ${}_{obs}\mathbf{E}_{IG}^{free}(f)$. Over all 2494 records, RMSLE are linear ~ 0.45, cubic ~ 0.40 and using Ardhuin et al. (2014) ~ 0.42. The free wave frequency distribution varies over a wide range and leads to relatively large RMSLE errors in all tested forms. NouvelleArdhuin (Eq. 9) is relatively simple, has the smallest errors, and is used below.

Timeseries realizations of the shoreward free IG are estimated from an inverse FFT of ${}_{pred}\mathbf{E}_{IG}^{free}(f)$,

$$\begin{aligned} {}_{p}\mathbf{E}_{IG}^{free}(f) &= {}_{p}E_{IG}^{free} * A(f), \\ {}_{p}E_{IG}^{free} &= 0.00067\tilde{\sigma} \textstyle\int_{SS} \mathbf{E}(f) f^{-1} df, \end{aligned} \tag{10}$$

with random phases and $A(f)$ (Eq. 9).

Linearly combining the computed bound wave timeseries with the estimated shoreward propagating free wave timeseries (with random phase), yields an estimated total shoreward IG timeseries that can be used as a boundary condition for numerical models. The parameterizations approximately reproduce a range of infragravity heights (Figure 6 c, RMSE ~ 0.01m, Model skill = 0.82, $R^2 = 0.95$, Bias = 0.006m).

4 Discussion

Ardhuin et al. (2014) parameterized seaward free IG energy as a function of local sea-swell conditions, and used that parameterization as a shoreline boundary condition in a global ocean wave model. The assumptions that seaward IG energy is free, directionally broad, and mainly radiated from the surfzone underlie the parameterization ${}_{p}\mathbf{E}_{IG}^{sea}(f)$

$${}_{p}\mathbf{E}_{IG}^{sea}(f) = \left[1.2\alpha^2 \frac{kg^2}{c_g 2\pi f} \left(\frac{H_s T_{m,0}^2}{4} \right)^2 \right] * \frac{1}{\Delta f} \left[\min\left(1, \frac{0.015\text{Hz}}{f}\right) \right]^{1.5}, \tag{11}$$

with the first part determining the frequency-band integrated ${}_{p}E_{IG}^{sea}$ energy, and the second, the frequency distribution of the seaward IG spectrum. Zheng et al. (2021) compared output from the Ardhuin et al. (2014) model and observations of H_{IG} and found $R^2 = 0.6$. This approach, for seaward IG energy, yields similar parameters for α ($= 6.6$ x $10^{-4} s^{-1}$) with $R^2 = 0.71$ between estimated and observed E_{IG}^{free} (Figure 7 a). A parameterization, similar to Eq. 8, for the seaward energy,

$${}_{p}E_{IG}^{seaward} = 0.001\tilde{\sigma} \int_{SS} \mathbf{E}(f) f^{-1} df. \tag{12}$$

shows similar tidal dependence of seaward and shoreward energy, and similar high skill $R^2 = 0.91$ (Figure 7 b). The ratio of seaward/shoreward = 0.001/0.00067 = 1.5, is constant and independent of tide. Although the dependencies on $\tilde{\sigma}$ and the constant are not well constrained, the implication that $\mathscr{R}_{IG}^2$ is not a function of tide level is supported by the low correlation ($R^2 = 0.22$) between tide and $\mathscr{R}_{IG}^2$ (Figure 8).

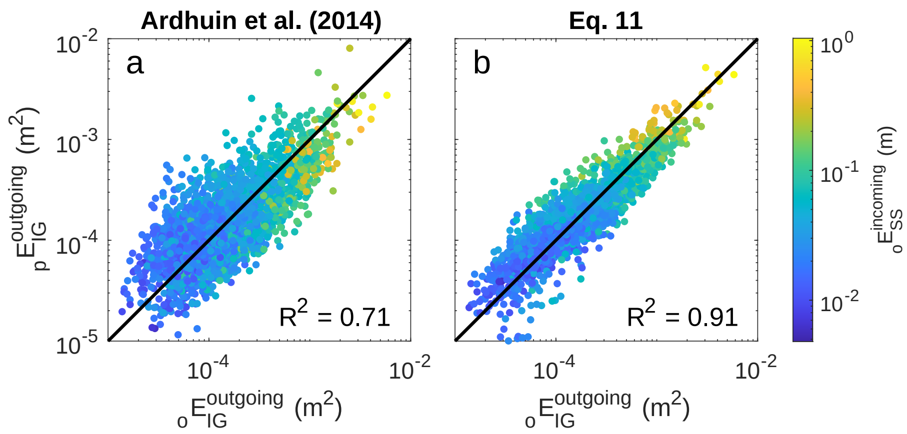

Figure 7. Parameterization of seaward IG energy from local SS conditions. (left) Ardhuin et al. (2014) ($R^2 = 0.71$) and (right) new parameterization ($R^2 = 0.91$), including tidal dependence (Eq. 12).

The observed total and free shoreward IG energy is tidally modulated(Figure 5 b, c), consistent with previous observations of total (seaward plus shoreward) IG energy in Southern California (Okihiro & Guza, 1995). This modulation, lower E_{IG} at low tide, has been attributed to IG energy loss within the surfzone being stronger on flat and shallow low-tide beaches than on steeper high-tide beaches (given a concave beach profile, Figure 8) (Thomson et al., 2006). Note that refractive trapping of seaward IG energy creates shoreward IG waves. That is, seaward and shoreward IG waves both increase at high tide, when the surfzone more efficiently radiates IG energy.

Observed values of $\mathscr{R}_{IG}^2$ vary between 0.5 - 2.5, whereas $\mathscr{R}_{IG}^2 = 1.5$ follows from the present crude parameterizations. While $\mathscr{R}_{IG}^2$ at the shoreline is constrained to < 1, $\mathscr{R}_{IG}^2 > 1$ in 10-15m depth can indicate IG surf zone generation and radiation, and shelf trapping. The ratio of free seaward to shoreward propagating IG energy in 10-15m depths is usually between 1 and 2. Along with the high correlation between E_{SS} and $_{obs}E_{IG}^{free}$, this suggests that between half and all of the energy radiated seaward is trapped on the shelf seaward of 10-15m and redirected shoreward (similar results seen in Gallagher, 1971; Elgar & Guza, 1985; Oltman-Shay & Guza, 1987; Okihiro et al., 1992; Elgar et al., 1992, 1994; Herbers & Guza, 1994; Herbers, Elgar, & Guza, 1995; Herbers, Elgar, Guza, & O'Reilly, 1995; Okihiro & Guza, 1995; Sheremet et al., 2002; Battjes, 2004; Thomson et al., 2006; S. M. Henderson et al., 2006; Rijnsdorp et al., 2015).

4.1 Numerical modelling of wave runup

The open-source, phase-resolving SWASH model (Zijlema et al., 2011) is used widely to simulate wave transformations and runup. SWASH successfully reproduces SS and IG evolution in laboratory channels with simple $h(x)$, and carefully controlled normally incident waves (A. de Bakker et al., 2014; Ruju et al., 2014; Suzuki et al., 2017). Field observations and model predictions of IG wave evolution and runup are also in good agreement, although limited by the relatively small range of conditions for which offshore boundary conditions (e.g. incident SS and IG waves), sandy beach bathymetry, and runup are all accurately known (Nicolae Lerma et al., 2017; Fiedler et al., 2018, 2019; Valentini et al., 2019; C. S. Henderson et al., 2022). For the current model runs, for computational reasons SWASH is run in nonstationary 2D mode in a narrow channel, with a curvilin-

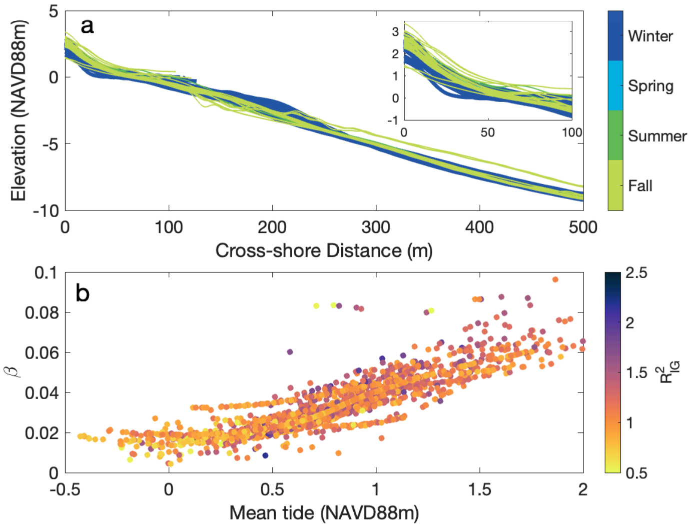

Figure 8. (a) Mean depth profiles at Torrey Pines (MOP 578 - 589), colored by season of survey. 85% of the 2209 surveys were collected in September/October/November ($n = 747$) and December/January/February ($n = 1125$). Insert shows subaerial beach. (b) Beach slope versus mean tide (relative to NAVD88m) of 3h record) at Torrey Pines. Beach slope is the linear fit ±0.5m around the tide level. The concave subaerial beach is steeper at high tide than low tide.

ear grid with a 2-m alongshore mesh for two identical parallel transects with 2 vertical layers. Waves are 1D. The normally incident wave field is prescribed with a Fourier series at the offshore boundary in 14m depth, about 600m from the shoreline. Parameter settings are as in Lange et al. (2022).

Significant IG growth and decay occurs during SS shoaling and breaking. Comparisons of runup with model run with $E_{IG} = 0$ and nouvelleArdhuin at the offshore boundary provide a measure of the effect of additional energy incident at the boundary. To test the relationship between incident IG energy in 10m and IG runup, we ran 23 wave cases of incident wave height ranging from $0.3 < H_{SS} < 4.1$m and $0.01 < H_{IG} < 0.44$m, with the IG boundary condition given by either $E_{IG} = 0$ or nouvelleArdhuin, and with the bathymetry profile either a 2-slope linear profile or an observed profile, for a total of 92 runs.

On the 2-slope profile, differences in runup with $E_{IG} = 0$ and nouvelleArdhuin are very small. On the observed bathymetry (derived from Figure 8 a), differences are detectable and best fit line slopes differ by about 15%. Consistent with linear intuition, runup is increased (modestly) by including incident IG waves at the offshore boundary. However, the cross-shore evolution of the shoreward IG waves is nonlinear and much more complicated than suggested by this simple example (Ruju et al., 2012; Fiedler et al., 2019; Mendes et al., 2018; Rijnsdorp et al., 2022). With steep test bathymetries and energetic wave conditions (not shown and not realistic in Southern California) $E_{IG} = 0$ can generate higher runup than nouvelleArduin, and effects of the offshore boundary condition on IG swash and runup can be significant (up to 20% different in the current cases and greater in cases run in Lange et al. (2022)).

We note that SWASH-modelled runup results were insensitive to different realizations of random phase in the simulations of free waves (not shown). Finally, SWASH-modelled seaward going IG energy in 10-15m was, for unknown reasons, significantly higher than the corresponding PUV observation (not shown), similar to C. S. Henderson et al.

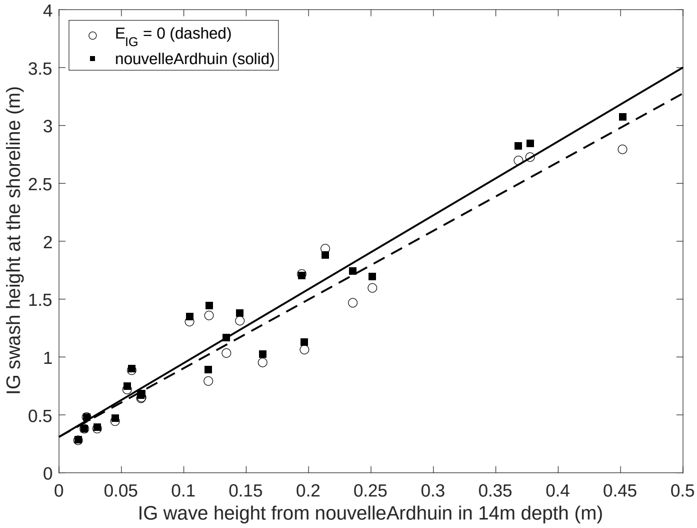

Figure 9. SWASH-modelled IG runup swash height versus nouvelleArdhuin offshore boundary condition IG height (∘, solid line is best fit). Runup is relatively insensitive to setting offshore $E_{IG} = 0$ (•, dashed). Best fit line slopes differ by 15% indicating a slight reduction in runup using $E_{IG} = 0$.

(2022). Possibly, errors arise because the SWASH 1D simulations assume normal wave incidence and do not support trapped waves. Simulations in 2D are beyond the present scope.

The applicability of the present results to other sites is unknown. Bound wave theory is general, not site-specific, and has no tunable parameters. However, the values of "free wave" parameters (Eqs. 6 and 10) are expected to vary with beach and shelf geometry. For example, the average depth of the North Sea is only 90m and slopes are low, potentially limiting the importance of refractive trapping relative to steeply sloped islands with deep water relatively close to shore (Rijnsdorp et al., 2021). The present sites are not between headlands or bounded by (fixed) offshore reefs. Selective amplification at particular IG frequencies has not been observed either in runup or on the inner shelf. Remotely generated IG waves from transoceanic sources are usually of relatively little importance. IG energy levels on the inner shelf depend on local waves and tide level. The numerical model result that IG wave runup at the shoreline is influenced only weakly by free IG waves on the inner shelf could significantly simplify overtopping forecasts by reducing the need for regional forecast models of IG waves.

5 Conclusion

The relative contribution of bound and free infragravity waves to the IG wave field on the inner shelf (depth $\sim 10-15$m) in San Diego County, USA was examined using PUV observations and nonlinear wave theory. In general, free waves dominate the IG wave field with only 5% of the records showing a bound wave fraction > 50%, consistent with previous observations in Southern California and Duck, USA and the North Sea. The bound wave energy scaled with the local SS energy squared (with higher correlation to swell energy than sea) and depth dependence is consistent with h^{-5} scaling. Free IG energy scaled linearly with the local SS energy and with the tide level.

These dependencies were included in parameterization of the total (bound and free IG) shoreward propagating energy that depen on tide level and wave models or buoy observations of SS waves. Parameterization of the seaward propagating IG waves showed a similar tidal dependence, differing from Ardhuin et al. (2014). Using an observation-based frequency distribution for free IG energy, bound and free wave are included in synthetic IG timeseries used to initialize the nonlinear, phase-resolving, numerical wave model SWASH. SWASH results suggest that wave runup is weakly influenced by free shoreward propagating IG waves observed at the offshore boundary.

Further observations and modeling are needed to extent the present results to other coastal locations.

Open Research Section

The 2494 timeseries of pressure, cross-shore and alongshore velocity is available on Zenodo at `https://doi.org/10.5281/zenodo.8254388`.

Acknowledgments

This study was funded by the U.S. Army Corps of Engineers (W912HZ1920020) and the California Department of Parks and Recreation (C19E0026). Data were collected and processed by the Coastal Processes Group field team members Lucian Parry, Rob Grenzeback, Kent Smith, Brian Woodward, Greg Boyd, Shane Finnerty, Carson Black, and Mele Johnson. Michele Okihiro organized logistics.

References

Aagaard, T., & Greenwood, B. (1994, April). Suspended sediment transport and the role of infragravity waves in a barred surf zone. *Marine Geology*, *118*(1-2), 23–48. Retrieved 2023-04-27, from `https://linkinghub.elsevier.com/retrieve/pii/0025322794901112` doi: 10.1016/0025-3227(94)90111-2

Aagaard, T., & Greenwood, B. (2008, May). Infragravity wave contribution to surf zone sediment transport — The role of advection. *Marine Geology*, *251*(1-2), 1–14. Retrieved 2023-04-27, from `https://linkinghub.elsevier.com/retrieve/pii/S0025322708000297` doi: 10.1016/j.margeo.2008.01.017

Altomare, C., Bolle, A., Brand, E., Chen, M., Dan, S., De Sloover, L., ... Zhange, Q. (2020). *CREST Final Scientific Report: Take Home Messages & Project Results.* VLIZ Special Publication 85.

Ardhuin, F., Devaux, E., & Pineau-Guillou, L. (2010). Observation et prévision des seiches sur la côte Atlantique française. In *XIèmes Journées, Les Sables d'Olonne* (pp. 1–8). Editions Paralia. Retrieved 2023-04-27, from `http://www.paralia.fr/jngcgc/11_01_ardhuin.pdf` doi: 10.5150/jngcgc.2010.001-A

Ardhuin, F., Rawat, A., & Aucan, J. (2014, May). A numerical model for free infragravity waves: Definition and validation at regional and global scales. *Ocean Modelling*, *77*, 20–32. Retrieved 2021-03-15, from `https://linkinghub.elsevier.com/retrieve/pii/S1463500314000274` doi: 10.1016/j.ocemod.2014.02.006

Baldock, T., Manoonvoravong, P., & Pham, K. S. (2010, October). Sediment transport and beach morphodynamics induced by free long waves, bound long waves and wave groups. *Coastal Engineering*, *57*(10), 898–916. Retrieved 2023-04-27, from `https://linkinghub.elsevier.com/retrieve/pii/S0378383910000694` doi: 10.1016/j.coastaleng.2010.05.006

Battjes, J. A. (2004). Shoaling of subharmonic gravity waves. *Journal of Geophysical Research*, *109*(C2), C02009. Retrieved 2019-05-13, from `http://doi.wiley.com/10.1029/2003JC001863` doi: 10.1029/2003JC001863

Behrens, J., Thomas, J., Terrill, E., & Jensen, R. (2019, March). CDIP: Maintaining a Robust and Reliable Ocean Observing Buoy Network. In

2019 IEEE/OES Twelfth Current, Waves and Turbulence Measurement (CWTM) (pp. 1–5). San Diego, CA, USA: IEEE. Retrieved 2023-04-06, from https://ieeexplore.ieee.org/document/8955166/ doi: 10.1109/CWTM43797.2019.8955166

de Bakker, A., Tissier, M., & Ruessink, B. (2014, January). Shoreline dissipation of infragravity waves. *Continental Shelf Research*, *72*, 73–82. Retrieved 2021-04-03, from https://linkinghub.elsevier.com/retrieve/pii/S0278434313003786 doi: 10.1016/j.csr.2013.11.013

De Bakker, A. T. M., Brinkkemper, J. A., Van Der Steen, F., Tissier, M. F. S., & Ruessink, B. G. (2016, October). Cross-shore sand transport by infragravity waves as a function of beach steepness: SAND TRANSPORT BY INFRAGRAVITY WAVES. *Journal of Geophysical Research: Earth Surface*, *121*(10), 1786–1799. Retrieved 2023-04-27, from http://doi.wiley.com/10.1002/2016JF003878 doi: 10.1002/2016JF003878

de Bakker, A. T. M., Herbers, T. H. C., Smit, P. B., Tissier, M. F. S., & Ruessink, B. G. (2015, February). Nonlinear Infragravity–Wave Interactions on a Gently Sloping Laboratory Beach. *Journal of Physical Oceanography*, *45*(2), 589–605. Retrieved 2021-04-03, from https://journals.ametsoc.org/view/journals/phoc/45/2/jpo-d-14-0186.1.xml doi: 10.1175/JPO-D-14-0186.1

Dusseljee, D., Klopman, G., Van Vledder, G., & Riezebos, H. J. (2014, December). IMPACT OF HARBOR NAVIGATION CHANNELS ON WAVES: A NUMERICAL MODELLING GUIDELINE. *Coastal Engineering Proceedings*, *1*(34), 58. Retrieved 2023-05-02, from https://journals.tdl.org/icce/index.php/icce/article/view/7710 doi: 10.9753/icce.v34.waves.58

Eckart, C. (1951). SURFACE WAVES ON WATER OF VARIABLE DEPTH.

Elgar, S., & Guza, R. T. (1985). Observations of bispectra of shoaling surface gravity waves. *Journal of Fluid Mechanics*.

Elgar, S., Herbers, T. H. C., & Guza, R. T. (1994, July). Reflection of Ocean Surface Gravity Waves from a Natural Beach. *Journal of Physical Oceanography*, *24*(7), 1503–1511. Retrieved 2023-04-30, from http://journals.ametsoc.org/doi/10.1175/1520-0485(1994)024<1503:ROOSGW>2.0.CO;2 doi: 10.1175/1520-0485(1994)024⟨1503:ROOSGW⟩2.0.CO;2

Elgar, S., Herbers, T. H. C., Okihiro, M., Oltman-Shay, J., & Guza, R. T. (1992). Observations of infragravity waves. , 5.

Elgar, S., Raubenheimer, B., & Guza, R. T. (2005, October). Quality control of acoustic Doppler velocimeter data in the surfzone. *Measurement Science and Technology*, *16*(10), 1889–1893. Retrieved 2023-04-11, from https://iopscience.iop.org/article/10.1088/0957-0233/16/10/002 doi: 10.1088/0957-0233/16/10/002

Fiedler, J. W., Smit, P. B., Brodie, K. L., McNinch, J., & Guza, R. (2018, January). Numerical modeling of wave runup on steep and mildly sloping natural beaches. *Coastal Engineering*, *131*, 106–113. Retrieved 2020-10-20, from https://linkinghub.elsevier.com/retrieve/pii/S037838391730193X doi: 10.1016/j.coastaleng.2017.09.004

Fiedler, J. W., Smit, P. B., Brodie, K. L., McNinch, J., & Guza, R. (2019, January). The offshore boundary condition in surf zone modeling. *Coastal Engineering*, *143*, 12–20. Retrieved 2019-08-14, from https://linkinghub.elsevier.com/retrieve/pii/S0378383918301984 doi: 10.1016/j.coastaleng.2018.10.014

Fiedler, J. W., Young, A. P., Ludka, B. C., O'Reilly, W. C., Henderson, C., Merrifield, M. A., & Guza, R. T. (2020, October). Predicting site-specific storm wave run-up. *Natural Hazards*, *104*(1), 493–517. Retrieved 2020-10-08, from http://link.springer.com/10.1007/s11069-020-04178-3 doi: 10.1007/s11069-020-04178-3

Gallagher, B. (1971, September). Generation of surf beat by non-linear wave interactions. *Journal of Fluid Mechanics*, *49*(1), 1–20. Retrieved 2021-03-01, from https://www.cambridge.org/core/product/identifier/S0022112071001897/type/journal_article doi: 10.1017/S0022112071001897

Guza, R. T., & Thornton, E. B. (1982). Swash oscillations on a natural beach. *Journal of Geophysical Research*, *87*(C1), 483. Retrieved 2020-06-08, from http://doi.wiley.com/10.1029/JC087iC01p00483 doi: 10.1029/JC087iC01p00483

Guza, R. T., & Thornton, E. B. (1985). Observations of surf beat. *Journal of Geophysical Research*, *90*(C2), 3161. Retrieved 2021-04-03, from http://doi.wiley.com/10.1029/JC090iC02p03161 doi: 10.1029/JC090iC02p03161

Hasselmann, K. (1962, April). On the non-linear energy transfer in a gravity-wave spectrum Part 1. General theory. *Journal of Fluid Mechanics*, *12*(04), 481. Retrieved 2020-10-08, from http://www.journals.cambridge.org/abstract_S0022112062000373 doi: 10.1017/S0022112062000373

Hasselmann, K., Munk, W. H., & MacDonald, G. (1963). *Bispectra of Ocean Waves.* Proc. of Time Series Analysis.

Henderson, C. S., Fiedler, J. W., Merrifield, M. A., Guza, R., & Young, A. P. (2022, August). Phase resolving runup and overtopping field validation of SWASH. *Coastal Engineering*, *175*, 104128. Retrieved 2023-04-06, from https://linkinghub.elsevier.com/retrieve/pii/S0378383922000436 doi: 10.1016/j.coastaleng.2022.104128

Henderson, S. M., Guza, R. T., Elgar, S., Herbers, T. H. C., & Bowen, A. J. (2006, December). Nonlinear generation and loss of infragravity wave energy. *Journal of Geophysical Research*, *111*(C12), C12007. Retrieved 2019-05-13, from http://doi.wiley.com/10.1029/2006JC003539 doi: 10.1029/2006JC003539

Herbers, T. H. C., Elgar, S., & Guza, R. T. (1995). Generation and propagation of infragravity waves. *Journal of Geophysical Research*, *100*(C12), 24863. Retrieved 2019-05-13, from http://doi.wiley.com/10.1029/95JC02680 doi: 10.1029/95JC02680

Herbers, T. H. C., Elgar, S., Guza, R. T., & O'Reilly, W. C. (1995). Infragravity-Frequency (0.005–0.05 Hz) Motions on the Shelf. Part II Free Waves. *Journal of Physical Oceanography*, 1063–1079.

Herbers, T. H. C., & Guza, R. T. (1994). Infragravity-Frequency (0.005–0.05 Hz) Motions on the Shelf. Part I Forced Waves. *Journal of Physical Oceanography*.

Huntley, D. A. (1976, December). Long-period waves on a natural beach. *Journal of Geophysical Research*, *81*(36), 6441–6449. Retrieved 2020-10-20, from http://doi.wiley.com/10.1029/JC081i036p06441 doi: 10.1029/JC081i036p06441

Huntley, D. A., Guza, R. T., & Thornton, E. B. (1981). Field observations of surf beat: 1. Progressive edge waves. *Journal of Geophysical Research*, *86*(C7), 6451. Retrieved 2021-03-02, from http://doi.wiley.com/10.1029/JC086iC07p06451 doi: 10.1029/JC086iC07p06451

Kim, Y. C., Beall, J. M., Powers, E. J., & Miksad, R. W. (1980). Bispectrum and nonlinear wave coupling. *Physics of Fluids*, *23*(2), 258. Retrieved 2019-06-01, from https://aip.scitation.org/doi/10.1063/1.862966 doi: 10.1063/1.862966

Kuik, A. (1988). *A Method for the Routine Analysis of Pitch-and-Roll Buoy Wave Data.* Journal of Physical Oceanography.

Lange, A. M., Fiedler, J. W., Becker, J. M., Merrifield, M. A., & Guza, R. (2022, March). Estimating runup with limited bathymetry. *Coastal Engineering*, *172*, 104055. Retrieved 2023-04-06, from https://linkinghub.elsevier.com/retrieve/pii/S0378383921001940 doi: 10.1016/j.coastaleng.2021.104055

Li, S., Liao, Z., Liu, Y., & Zou, Q. (2020, August). Evolution of Infragravity Waves Over a Shoal Under Nonbreaking Conditions. *Journal of Geophysical Research: Oceans*, *125*(8). Retrieved 2023-05-02, from https://onlinelibrary.wiley.com/doi/10.1029/2019JC015864 doi: 10.1029/2019JC015864

List, J. H. (1986). Wave Groupiness as a Source of Nearshore Long Waves. *COASTAL ENGINEERING*, 15.

Longuet-Higgins, M. S., & Stewart, R. W. (1962, August). Radiation stress and mass transport in gravity waves, with application to 'surf beats'. *Journal of Fluid Mechanics*, *13*(4), 481–504. Retrieved 2019-05-13, from https://www.cambridge.org/core/product/identifier/S0022112062000877/type/journal_article doi: 10.1017/S0022112062000877

Ludka, B. C., Guza, R. T., O'Reilly, W. C., Merrifield, M. A., Flick, R. E., Bak, A. S., ... Boyd, G. (2019, December). Sixteen years of bathymetry and waves at San Diego beaches. *Scientific Data*, *6*(1), 161. Retrieved 2020-07-27, from http://www.nature.com/articles/s41597-019-0167-6 doi: 10.1038/s41597-019-0167-6

Mendes, D., Pinto, J. P., Pires-Silva, A. A., & Fortunato, A. B. (2018, October). Infragravity wave energy changes on a dissipative barred beach: A numerical study. *Coastal Engineering*, *140*, 136–146. Retrieved 2023-07-25, from https://linkinghub.elsevier.com/retrieve/pii/S0378383918300322 doi: 10.1016/j.coastaleng.2018.07.005

Munk, W. H. (1949). Surf beats. *Transactions, American Geophysical Union*, *30*(6), 849. Retrieved 2019-05-28, from http://doi.wiley.com/10.1029/TR030i006p00849 doi: 10.1029/TR030i006p00849

Nicolae Lerma, A., Pedreros, R., Robinet, A., & Sénéchal, N. (2017, May). Simulating wave setup and runup during storm conditions on a complex barred beach. *Coastal Engineering*, *123*, 29–41. Retrieved 2023-04-06, from https://linkinghub.elsevier.com/retrieve/pii/S0378383916301284 doi: 10.1016/j.coastaleng.2017.01.011

Okihiro, M., & Guza, R. T. (1995). Infragravity energy modulation by tides. *Journal of Geophysical Research*, *100*(C8), 16143. Retrieved 2021-03-12, from http://doi.wiley.com/10.1029/95JC01545 doi: 10.1029/95JC01545

Okihiro, M., Guza, R. T., & Seymour, R. J. (1992). Bound Infragravity Waves. *Journal of Geophysical Research*, *97*(C7), 11453–11469. Retrieved 2021-03-01, from http://doi.wiley.com/10.1029/92JC00270 doi: 10.1029/92JC00270

Okihiro, M., Guza, R. T., & Seymour, R. J. (1993). Excitation of seiche observed in a small harbor. *Journal of Geophysical Research*, *98*(C10), 18201. Retrieved 2023-04-30, from http://doi.wiley.com/10.1029/93JC01760 doi: 10.1029/93JC01760

Oltman-Shay, J., & Guza, R. T. (1987). *Infragravity Edge Wave Observations on Two California Beaches.pdf.* Journal of Physical Oceanography.

Oltman-Shay, J., & Howd, P. A. (1993, February). Edge waves on nonplanar bathymetry and alongshore currents: A model and data comparison. *Journal of Geophysical Research: Oceans*, *98*(C2), 2495–2507. Retrieved 2023-04-27, from http://doi.wiley.com/10.1029/92JC02609 doi: 10.1029/92JC02609

O'Reilly, W., Olfe, C. B., Thomas, J., Seymour, R., & Guza, R. (2016, October). The California coastal wave monitoring and prediction system. *Coastal Engineering*, *116*, 118–132. Retrieved 2019-08-14, from https://linkinghub.elsevier.com/retrieve/pii/S0378383916301120 doi: 10.1016/j.coastaleng.2016.06.005

Qin, L., & Li, Y. (2021, November). Significant Wave Height Estimation Using Multi-Satellite Observations from GNSS-R. *Remote Sensing*, *13*(23), 4806. Retrieved 2023-04-27, from https://www.mdpi.com/2072-4292/13/23/4806 doi: 10.3390/rs13234806

Rawat, A., Ardhuin, F., Ballu, V., Crawford, W., Corela, C., & Aucan, J. (2014, November). Infragravity waves across the oceans: Following Infra-Gravity Wave Bursts. *Geophysical Research Letters*, *41*(22), 7957–7963. Retrieved 2021-04-02, from http://doi.wiley.com/10.1002/2014GL061604 doi: 10.1002/2014GL061604

Reniers, A. J., Naporowski, R., Tissier, M. F. S., de Schipper, M. A., Akrish, G., & Rijnsdorp, D. P. (2021, January). North Sea Infragravity Wave Observations. *Journal of Marine Science and Engineering*, *9*(2), 141. Retrieved 2021-04-02, from `https://www.mdpi.com/2077-1312/9/2/141` doi: 10.3390/jmse9020141

Reniers, A. J. H. M. (2002). Linear modeling of infragravity waves during Delilah. *Journal of Geophysical Research*, *107*(C10), 3137. Retrieved 2021-04-02, from `http://doi.wiley.com/10.1029/2001JC001083` doi: 10.1029/2001JC001083

Rhie, J., & Romanowicz, B. (2006, October). A study of the relation between ocean storms and the Earth's hum: OCEAN STORMS AND EARTH'S HUM. *Geochemistry, Geophysics, Geosystems*, *7*(10), n/a–n/a. Retrieved 2023-04-27, from `http://doi.wiley.com/10.1029/2006GC001274` doi: 10.1029/2006GC001274

Ribal, A., & Young, I. R. (2019, May). 33 years of globally calibrated wave height and wind speed data based on altimeter observations. *Scientific Data*, *6*(1), 77. Retrieved 2023-04-27, from `https://www.nature.com/articles/s41597-019-0083-9` doi: 10.1038/s41597-019-0083-9

Rijnsdorp, D. P., Reniers, A. J. H. M., & Zijlema, M. (2021, August). Free Infragravity Waves in the North Sea. *Journal of Geophysical Research: Oceans*, *126*(8). Retrieved 2023-04-06, from `https://onlinelibrary.wiley.com/doi/10.1029/2021JC017368` doi: 10.1029/2021JC017368

Rijnsdorp, D. P., Ruessink, G., & Zijlema, M. (2015, June). Infragravity-wave dynamics in a barred coastal region, a numerical study. *Journal of Geophysical Research: Oceans*, *120*(6), 4068–4089. Retrieved 2021-04-02, from `https://onlinelibrary.wiley.com/doi/abs/10.1002/2014JC010450` doi: 10.1002/2014JC010450

Rijnsdorp, D. P., Smit, P. B., & Guza, R. (2022, August). A nonlinear, non-dispersive energy balance for surfzone waves: infragravity wave dynamics on a sloping beach. *Journal of Fluid Mechanics*, *944*, A45. Retrieved 2023-07-25, from `https://www.cambridge.org/core/product/identifier/S0022112022005122/type/journal_article` doi: 10.1017/jfm.2022.512

Rijnsdorp, D. P., Smit, P. B., & Zijlema, M. (2014, March). Non-hydrostatic modelling of infragravity waves under laboratory conditions. *Coastal Engineering*, *85*, 30–42. Retrieved 2023-05-02, from `https://linkinghub.elsevier.com/retrieve/pii/S0378383913001944` doi: 10.1016/j.coastaleng.2013.11.011

Roelvink, D., Reniers, A., Van Dongeren, A., Van Thiel De Vries, J., McCall, R., & Lescinski, J. (2009, November). Modelling storm impacts on beaches, dunes and barrier islands. *Coastal Engineering*, *56*(11-12), 1133–1152. Retrieved 2023-05-02, from `https://linkinghub.elsevier.com/retrieve/pii/S0378383909001252` doi: 10.1016/j.coastaleng.2009.08.006

Ruessink, B. G. (1998, June). Bound and free infragravity waves in the nearshore zone under breaking and nonbreaking conditions. *Journal of Geophysical Research: Oceans*, *103*(C6), 12795–12805. Retrieved 2019-05-13, from `http://doi.wiley.com/10.1029/98JC00893` doi: 10.1029/98JC00893

Ruessink, G., Michallet, H., Bonneton, P., Mouazé, D., Lara, J. L., Silva, P. A., & Wellens, P. (2013). GLOBEX: WAVE DYNAMICS ON A GENTLY SLOPING LABORATORY BEACH. *Coastal Dynamics*, 12.

Ruggiero, P. (2004). Wave run-up on a high-energy dissipative beach. *Journal of Geophysical Research*, *109*(C6), C06025. Retrieved 2021-03-12, from `http://doi.wiley.com/10.1029/2003JC002160` doi: 10.1029/2003JC002160

Ruju, A., Lara, J. L., & Losada, I. J. (2012, October). Radiation stress and low-frequency energy balance within the surf zone: A numerical approach. *Coastal Engineering*, *68*, 44–55. Retrieved 2023-04-30, from `https://linkinghub.elsevier.com/retrieve/pii/S0378383912000907` doi: 10.1016/j.coastaleng.2012.05.003

Ruju, A., Lara, J. L., & Losada, I. J. (2014, April). Numerical analysis of run-up oscillations under dissipative conditions. *Coastal Engineering*, *86*, 45–56. Retrieved 2020-10-08, from https://linkinghub.elsevier.com/retrieve/pii/S0378383914000192 doi: 10.1016/j.coastaleng.2014.01.010

Sand, S. E. (1982, January). Wave grouping described by bounded long waves. *Ocean Engineering*, *9*(6), 567–580. Retrieved 2021-03-01, from https://linkinghub.elsevier.com/retrieve/pii/0029801882900038 doi: 10.1016/0029-8018(82)90003-8

Sheremet, A., Guza, R. T., Elgar, S., & Herbers, T. H. C. (2002). Observations of nearshore infragravity waves: Seaward and shoreward propagating components. *Journal of Geophysical Research*, *107*(C8), 3095. Retrieved 2021-03-12, from http://doi.wiley.com/10.1029/2001JC000970 doi: 10.1029/2001JC000970

Smit, P. B., Janssen, T. T., Herbers, T. H. C., Taira, T., & Romanowicz, B. A. (2018, July). Infragravity Wave Radiation Across the Shelf Break. *Journal of Geophysical Research: Oceans*, *123*(7), 4483–4490. Retrieved 2023-04-30, from https://onlinelibrary.wiley.com/doi/10.1029/2018JC013986 doi: 10.1029/2018JC013986

Stockdon, H. F., Holman, R. A., Howd, P. A., & Sallenger, A. H. (2006, May). Empirical parameterization of setup, swash, and runup. *Coastal Engineering*, *53*(7), 573–588. Retrieved 2020-03-17, from https://linkinghub.elsevier.com/retrieve/pii/S0378383906000044 doi: 10.1016/j.coastaleng.2005.12.005

Suzuki, T., Altomare, C., Veale, W., Verwaest, T., Trouw, K., Troch, P., & Zijlema, M. (2017, April). Efficient and robust wave overtopping estimation for impermeable coastal structures in shallow foreshores using SWASH. *Coastal Engineering*, *122*, 108–123. Retrieved 2020-10-20, from https://linkinghub.elsevier.com/retrieve/pii/S0378383916302435 doi: 10.1016/j.coastaleng.2017.01.009

Thomson, J., Elgar, S., Raubenheimer, B., Herbers, T. H. C., & Guza, R. T. (2006). Tidal modulation of infragravity waves via nonlinear energy losses in the surfzone. *Geophysical Research Letters*, *33*(5), L05601. Retrieved 2019-05-16, from http://doi.wiley.com/10.1029/2005GL025514 doi: 10.1029/2005GL025514

Tucker, M. (1950, August). Surf beats: sea waves of 1 to 5 min. period. *Proceedings of the Royal Society of London. Series A. Mathematical and Physical Sciences*, *202*(1071), 565–573. Retrieved 2021-02-26, from https://royalsocietypublishing.org/doi/10.1098/rspa.1950.0120 doi: 10.1098/rspa.1950.0120

Valentini, N., Saponieri, A., Danisi, A., Pratola, L., & Damiani, L. (2019, September). Exploiting remote imagery in an embayed sandy beach for the validation of a runup model framework. *Estuarine, Coastal and Shelf Science*, *225*, 106244. Retrieved 2023-07-25, from https://linkinghub.elsevier.com/retrieve/pii/S0272771418310333 doi: 10.1016/j.ecss.2019.106244

van Dongeren, A., Battjes, J., Janssen, T., van Noorloos, J., Steenhauer, K., Steenbergen, G., & Reniers, A. (2007, February). Shoaling and shoreline dissipation of low-frequency waves. *Journal of Geophysical Research*, *112*(C2), C02011. Retrieved 2019-05-13, from http://doi.wiley.com/10.1029/2006JC003701 doi: 10.1029/2006JC003701

van Noorloos, J. C. (2003). Energy transfer between short wave groups and bound long waves on a plane slope.

Van Thiel De Vries, J., Van Gent, M., Walstra, D., & Reniers, A. (2008, December). Analysis of dune erosion processes in large-scale flume experiments. *Coastal Engineering*, *55*(12), 1028–1040. Retrieved 2023-05-02, from https://linkinghub.elsevier.com/retrieve/pii/S0378383908000860 doi: 10.1016/j.coastaleng.2008.04.004

Webb, S. C. (2007, February). The Earth's 'hum' is driven by ocean waves over the continental shelves. *Nature*, *445*(7129), 754–756. Retrieved 2023-04-30, from http://www.nature.com/articles/nature05536 doi: 10.1038/nature05536

Webb, S. C., Zhang, X., & Crawford, W. (1991). Infragravity waves in the deep ocean. , 14.

Zhang, Q., Toorman, E. A., & Monbaliu, J. (2020, June). Shoaling of bound infragravity waves on plane slopes for bichromatic wave conditions. *Coastal Engineering*, *158*, 103684. Retrieved 2023-05-02, from https://linkinghub.elsevier.com/retrieve/pii/S037838391930198X doi: 10.1016/j.coastaleng.2020.103684

Zheng, Z., Ma, X., Ma, Y., Huang, X., & Dong, G. (2021, December). Modeling of coastal infragravity waves using the spectral model WAVEWATCH . *Coastal Engineering*, *170*, 104016. Retrieved 2023-04-20, from https://linkinghub.elsevier.com/retrieve/pii/S0378383921001654 doi: 10.1016/j.coastaleng.2021.104016

Zijlema, M. (2012, October). MODELLING WAVE TRANSFORMATION ACROSS A FRINGING REEF USING SWASH. *Coastal Engineering Proceedings*, *1*(33), 26. Retrieved 2020-07-14, from https://icce-ojs-tamu.tdl.org/icce/index.php/icce/article/view/6479 doi: 10.9753/icce.v33.currents.26

Zijlema, M., Stelling, G., & Smit, P. (2011, October). SWASH: An operational public domain code for simulating wave fields and rapidly varied flows in coastal waters. *Coastal Engineering*, *58*(10), 992–1012. Retrieved 2020-10-08, from https://linkinghub.elsevier.com/retrieve/pii/S0378383911000974 doi: 10.1016/j.coastaleng.2011.05.015